Effects of seasonal variations in vegetation and precipitation on catchment erosion rates along a climate and ecological gradient: Insights from numerical modelling

Hemanti Sharma[1] and Todd A. Ehlers[1,2]

[1]Department of Geosciences, University of Tübingen, Schnarrenbergstr. 94-96, 72076, Germany

[2]School of Geographical and Earth Sciences, University of Glasgow, Glasgow, Scotland

Correspondence to: Todd A. Ehlers (todd.ehlers@uni-tuebingen.de)

Abstract. Precipitation in wet seasons influences catchment erosion and contributes to annual erosion rates. However, wet seasons are also associated with increased vegetation cover, which helps resist erosion. This study investigates the effect of present-day seasonal variations in rainfall and vegetation cover on erosion rates for four catchments along the extreme climate and ecological gradient (from arid to temperate) of the Chilean Coastal Cordillera (~26 °S – ~38 °S). We do this using the Landlab-SPACE landscape evolution model using a set of runtime scripts and input files to account for vegetation-dependent hillslope-fluvial processes and hillslope hydrology. Model inputs include present-day (90 m) topography, and a timeseries (from 2000-2019) of MODIS-derived NDVI for vegetation seasonality; weather station observations of precipitation; and evapotranspiration obtained from GLDAS NOAH. Simulations were conducted with a step-wise increase in complexity to quantify the sensitivity of catchment scale erosion rates to seasonal average variations in precipitation and/or vegetation cover. Simulations were conducted for 1,000 years (20 years of vegetation and precipitation observations repeated 50 times). After detrending the results for long-term transient changes, the last 20 years were analyzed. Results indicate that when vegetation cover is variable but precipitation is held constant, the amplitude of change in erosion rates relative to mean erosion rates ranges between 5% (arid) to 36% (Mediterranean setting). In contrast, in simulations with variable precipitation change and constant vegetation cover, the amplitude of change in erosion rates is higher and ranges between 13% (arid) to 91% (Mediterranean setting). Finally, simulations with coupled precipitation and vegetation cover variations demonstrate variations in catchment erosion of 13% (arid) to 97% (Mediterranean setting). Taken together, we find that precipitation variations more strongly influence seasonal variations in erosion rates. However, the effects of seasonal variations in vegetation cover on erosion are also significant (between 5-36%) and are most pronounced in semi-arid to Mediterranean settings and least prevalent in arid and humid-temperature settings.

Keywords: Landlab, vegetation, Chilean Coastal Cordillera, biogeomorphology, seasonality, precipitation, EarthShape.

1 Introduction

Catchment erosion rates vary spatially and temporally (e.g., Wang et al., 2021) and depend on topography (slope, Carretier et al., 2018), vegetation cover and type (e.g., Zhang et al., 2011; Starke et al., 2020; Schaller and Ehlers, 2022) and precipitation rates (e.g., Cerdà, 1998; Tucker and Bras, 2000). Over annual timescales, temporal variations in catchment erosion occur in response to seasonal variations in precipitation and vegetation cover. For example, previous work has found that a significant fraction of annual erosion occurs during wet seasons, with high runoff rates (Hancock and Lowry, 2021; Leyland et al., 2016; Gao et al., 2021; Wulf et al., 2010). However, this increase in precipitation during wet seasons also promotes vegetation growth, which in turn influences erosion rates (Langbein and Schumm, 1958; Zheng, 2006; Schmid et al., 2018). Seasonal and longer-term changes in both precipitation and vegetation cover play a crucial role in intra-annual changes in erosion rates (Istanbulluoglu and Bras, 2006; Yetemen et al., 2015; Schmid et al., 2018; Sharma et al., 2021). The intensity, frequency, and

Deleted: modified
Formatted
Deleted: varied
Deleted: 6.
Deleted: humid-temperate
Deleted: Seasonality,
Deleted: ,
Deleted: plays

seasonality of precipitation and vegetation cover change within a year depend upon the climate and ecological conditions of the area of interest (Herrmann and Mohr, 2011). One means of investigating the effects of seasonality in precipitation and (or) vegetation cover on erosion rates is through landscape evolution modeling (LEM), which can be parameterized for variations in vegetation-dependent hillslope and fluvial processes over seasonal time scales.

Previous modeling and observational studies have investigated the effects of seasonality in precipitation and vegetation on catchment erosion. Bookhagen et al., (2005), Wulf et al., (2010), and Deal et al., (2017) investigated the effects of stochastic variations in precipitation on erosion and sediment transport in the Himalayas. They found that high variability in rainstorm days (>80% of MAP) during the wet season (summer monsoon) caused high variability in the suspended sediment load. Similar seasonality in sediment loads was reported in a field study in Iran, using sediment traps and erosion pins. These authors concluded that wet seasons experienced maximum erosion rates (>70% of annual), which decreased in dry seasons (<10% of annual) (Mosaffaie et al., 2015). Field observations in the heavily vegetated Columbian Andes concluded that soil erosion and nutrient losses are significantly influenced by precipitation seasonality (Suescún et al., 2017). In contrast, work by Steegen et al., (2000) in a loamy agricultural catchment in central Belgium found suspended sediment concentrations in streams were lower during summer (wet) rather than winter (dry) months due to the development in vegetation cover in the wet season. Other workers have found a dependence of seasonal erosion on ecosystem type. For example, Istanbulluoglu et al., (2006) found a reduction in the sensitivity of soil loss potential to storm frequency in humid ecosystems compared to arid and semi-arid regions. Work by Wei et al., (2015) in the semi-arid setting of the Chinese Loess Plateau, reported that significant changes in vegetation related land use/land cover may contribute to long-term soil loss dynamics. However, seasonal variations in runoff and sediment yield are mainly influenced by intra-annual rainfall variations. Finally, previous work in a Mediterranean environment by Gabarrón-Galeote et al., (2013), described rainfall intensity as the main factor in determining hydrological erosive response, regardless of the rainfall depth of an event.

When looking at seasonal vegetation changes in more detail, several different studies suggest these changes are important for catchment erosion. For example, Garatuza-Payán et al., (2005) emphasized that seasonal patterns in erosion are strongly influenced by plant phenology as demonstrated by the changes in vegetation cover (measured by NDVI). A similar study on the Loess Plateau, China, by Zheng (2006) documented decreasing soil erosion as vegetation cover increases during the wet season. Work conducted in a forested setting (Zhang et al., 2014) documented the importance of tree cover as an effective filter for decreasing the effects of rainfall intensity on soil structure, runoff, and sediment yield. Numerical modeling studies have also found a significant impact of vegetation on erosion. For example, Zhang et al., (2019) found that when precipitation was kept constant, the increase in vegetation cover resulted in a significant reduction in sediment yields (20-30% of the total flux). Also, during early to mid-wet season, the species richness and evenness of plant cover both play an essential role in reducing erosion rates during low rainfall events (Hou et al., 2020). However, in the case of high-intensity rainfall events at the start of a wet season, when vegetation cover is low, the duration and intensity of rainfall were found to significantly affect erosion rates (Hancock and Lowry, 2015). Other work conducted in a Mediterranean environment points to the coincidence of peak rainfall erosivity in low vegetation cover settings, leading to an increased risk of soil erosion (Ferreira and Panagopoulos, 2014). Despite potentially conflicting results in the previous studies, what is clear is that seasonality in precipitation and vegetation cover conspire to influence catchment erosion, although which factor (precipitation or vegetation) plays the dominant role is unclear.

This study complements the previous work by applying a Landscape Evolution Model (LEM) to investigate seasonal transience in catchment erosion due to variations in precipitation and vegetation. We do this for four locations spanning the extreme climate and ecological gradient (i.e., arid, semi-arid, Mediterranean, and humid temperate) in the Chilean Coastal Cordillera. Our efforts are focused on testing two hypotheses: (1) precipitation is the first-order driver of seasonal erosion rates, and (2) catchment erosion in arid and semi-arid regions is more sensitive to seasonality in precipitation and vegetation than the

Deleted: on

Field Code Changed

Field Code Changed

Deleted: Work by Chakrapani (2005) identifies the control of mean local relief and seasonality in precipitation on sediment load in rivers. Similar seasonality in sediment loads was reported in a field study in Iran, using sediment traps and erosion pins.

Deleted: have

Deleted: decreases

Deleted: the

Deleted: season

Deleted: documented

Deleted: differences

Deleted: erosion and sedimentation

Deleted: (

Deleted: as

Deleted: is

Deleted: effect of

Deleted: change on

Deleted: is significant

Deleted: the

Deleted: the

Deleted: covers are co-

Deleted: transients

Deleted: in

Deleted: of

Deleted: if

Deleted: , then the influence of seasonal changes in vegetation cover would be of low significance

Mediterranean and humid temperate regions. To test the above hypotheses, we conduct a sensitivity analysis of fluvial and hillslope erosion over four Chilean study areas to investigate the individual effects of seasonal changes in vegetation cover and precipitation compared to simulations with coupled variations in precipitation and vegetation cover. We do this using a two-dimensional LEM (the Landlab-SPACE software), which explicitly handles bedrock and sediment entrainment and deposition. We build upon the approach of Sharma et al., (2021) with the additional consideration of soil-water infiltration. Our model setup broadly representative of the present-day conditions in the Chilean Coastal Cordillera (Fig. 1) and uses present-day inputs such as topography from SRTM DEMs (90 m) for four regions with different climate/ecological settings. Simulations in these different ecosystems are driven by observed variations in vegetation cover from MODIS NDVI (between 2000 – 2019) and observed precipitation rates over the same time period from neighboring weather stations. We note that the aim of this study is not to reproduce reality in these study areas. This is due to the uncertainties in the LEM initial conditions and material properties, and rock uplift rates. Rather, our focus is a series of sensitivity analyses that are loosely 'tuned' to natural conditions and observed vegetation and precipitation changes along an ecological gradient. As shown below, these simplifications facilitate identifying the relative contributions of vegetation and precipitation changes on catchment erosion.

Deleted: is focused on

Deleted: use as input

Deleted:

Deleted: drive

2 Study Areas

This section summarizes the geologic, climate, and vegetation settings of the four selected catchments (Fig. 1) investigated in the Chilean Coastal Cordillera. These catchments (from north to south) are located in the Pan de Azúcar National Park (arid, ~26°S), Santa Gracia Nature Reserve (semi-arid, ~30°S), and the La Campana (Mediterranean, ~33°S) and Nahuelbuta (temperate-humid, ~38°S) national parks. Together, these study areas span ~1,300 km distance of the Coastal Cordillera. These study areas are chosen for their steep climate and ecological gradient from north (arid environment with small to no shrubs) to south (humid temperate environment with evergreen mixed forests) (Schaller et al., 2020). The study areas are part of the German-Chilean priority research program EarthShape (www.earthshape.net) and ongoing research efforts within these catchments.

Deleted: nature preserve

Deleted: mediterranean

Deleted: North

Deleted: South

Field Code Changed

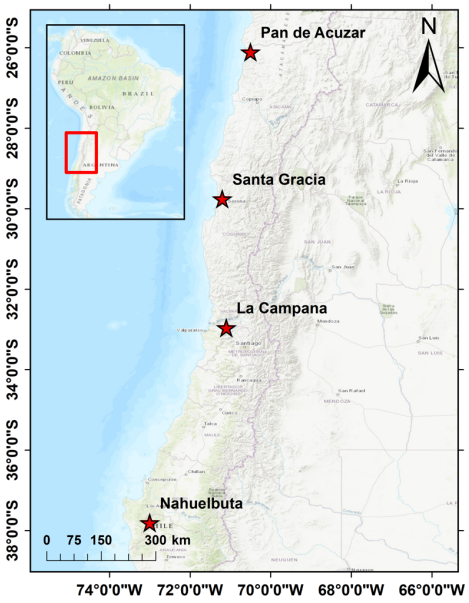

Figure 1. Study areas in the Coastal Chilean Cordillera ranging from an arid environment in the north (Pan de Azúcar), semi-arid (Santa Gracia), Mediterranean (La Campana), and humid temperate environment in the south (Nahuelbuta). The above map is obtained from the Environmental System Research Institute (ESRI) map server (https://services.arcgisonline.com/ArcGIS/rest/services/World_Topo_Map/MapServer, last access: 25 April 2022).

The bedrock of the four study areas is composed of granitoid rocks, including granites, granodiorites, and tonalites in Pan de Azúcar, La Campana, and Nahuelbuta, respectively, and gabbro and diorites in Santa Gracia (Oeser et al., 2018). The soil types in each catchment were identified as a sandy loam in three northern catchments (with high bulk density: 1300 – 1500 kg m^{-3}) and sandy clay loam in Nahuelbuta (with lower bulk density: 800 kg m^{-3}) (Bernhard et al., 2018). The western margin of Chile along the latitudes of the different study areas is characterized by a similar tectonic setting whereby an oceanic plate (currently the Nazca Plate) has been subducting under the South American Plate since the Palaeozoic. Despite this common tectonic setting along, slight differences in modern rock uplift rates are documented in the regions surrounding the three northern catchments (i.e., < 0.1 mm yr^{-1} for ~ 26 °S to ~33 °S) (Melnick, 2016) and the southern catchment (i.e., 0.04 to > 0.2 mm yr^{-1} for ~38 °S over the last 4±1.2 Ma) (Glodny et al., 2008; Melnick et al., 2009). Over geologic (millennial) timescales, measured denudation rates in the region range between ~0.005 to ~0.6 mm yr^{-1} (Schaller et al., 2018). To facilitate a comparison between the study areas and focus on erosion variations from seasonal changes in precipitation and vegetation, we assume a uniform rock uplift rate of 0.05 mm yr^{-1} for this study. This rate is broadly consistent with the range of previously reported values.

The climate gradient in the study areas ranges from an arid climate in Pan de Azúcar (north) with mean annual precipitation (MAP) of ~11 mm yr^{-1} to semi-arid in Santa Gracia (MAP: ~ 88 mm yr^{-1}), a Mediterranean climate in La Campana (MAP: ~350 mm yr^{-1}), and a temperate-humid climate in Nahuelbuta (south) with a MAP of 1400 mm yr^{-1} (Ziese et al., 2020). The observed mean annual temperatures (MAT) also vary with latitude ranging from ~20°C in the north to ~5°C in the south (Übernickel et al., 2020). The previous gradients in MAP and MAT and latitudinal variations in solar radiation result in a

Deleted: North
Deleted: South
Field Code Changed
Deleted: plate
Deleted: plate
Deleted: the

southward increase in vegetation density (Bernhard et al., 2018). The vegetation gradient is evident from mean MODIS Normalized Difference Vegetation Index (NDVI) values range from ~0.1 in Pan de Azúcar (north) to ~0.8 in Nahuelbuta (south) (Didan, Kamel, 2015). In this study, NDVI values are used as a proxy for vegetation cover density, similar to the approach of Schmid et al. (2018). However, one of the major limitations of using NDVI is that the values get saturated when the ground is covered by shrubs. This gradient in climate and vegetation cover from north to south in the Chilean Coastal Cordillera provides an opportunity to study the effects of seasonal variations in vegetation cover and precipitation on catchment-scale erosion rates in different environments.

3 Methods

This section comprises a description of model inputs (section 3.1), estimation of runoff rates (section 3.2), model setup (section 3.3), and initial and boundary conditions (section 3.4). This is followed by an overview of simulations conducted (section 3.5), and a brief description of how detrending the model results was conducted to remove long-term transients (section 3.6).

3.1 Data used for model inputs

In contrast to previous modeling studies (Schmid et al., 2018; Sharma et al., 2021) in the same regions, we used present-day topography as the initial condition for simulations instead of a synthetic topography produced during a model spin-up phase in Landlab. This study focuses on predicting and comparing the average responses in catchment erosion that occur over seasonal timescales with variable precipitation and vegetation cover. However, erosion in arid and semi-arid regions can vary on sub-seasonal time scales due to high-intensity storms occurring over timescales of a couple of hours or days. Hence, the model does not capture the role of extreme precipitation events. The effect of vegetation on erosion during extreme events is the focus of ongoing work by the authors. Also, at seasonal time-steps, the relationship between vegetation cover and erosion rates may be affected by inherited simulated slope values from the previous season, which may lead to the blended signal in the output.

Initial topography for the four selected catchments was obtained by cropping the SRTM digital elevation model (DEM) in rectangular shapes encapsulating the catchment of interest (Fig. 1). These catchments are the same as those investigated with previous soil, denudation, and geophysical studies within the EarthShape project (e.g., Bernhard et al., 2018; Oeser et al., 2018; Schaller et al., 2018; Dal Bo et al., 2019). The DEM has a spatial resolution of 90 m and is the same as the cell size used in the model (dx and dy) (SRTM data set of Earth Resources Observation And Science (EROS) Center, 2017). The present-day total relief in the catchments are ~1852 m in La Campana (~33 °S), followed by ~1063 m in Santa Gracia (~30 °S), ~809 m in Nahuelbuta (~38 °S) and ~623 m Pan de Azúcar (~26 °S). Investigated catchment sizes considered here vary between ~64 km^2 in Pan de Azúcar, ~142.5 km^2 in Santa Gracia, ~106.8 km^2 in La Campana, and ~68.7 km^2 in Nahuelbuta. We note that present-day topography as the initial condition in simulations can introduce an initial transience in erosion rates due to assumed model erosional parameters (e.g., erodibility, hillslope diffusivity) differing from actual parameters within the catchment. We address this issue through a detrending of model results described later (see Section 3.6). Also, topography and processes represented by LEMs have inherent timescales that they respond to base on the physical properties used and model forcings (e.g., rock uplift), which are unknown. Hence, it is unlikely that the SRTM DEM used for the initial condition, is in equilibrium. Given this, the detrending of our time series of results to remove long-term transience aids in identifying seasonal transients in precipitation and vegetation cover.

Precipitation data applied over each study area (Fig. 3b) was acquired from the Global Precipitation Climatology Centre (GPCC) for the period 01/03/2000 to 31/12/2019 (DD/MM/YEAR). The data has a spatial resolution of 1° and a 1-day temporal resolution and comprises daily land-surface precipitation from rain gauges built on Global Telecommunication System-based

Deleted: LandLab.

Deleted:)/

Deleted: Maximum

Deleted: of

Deleted: is observed

Deleted: Catchment

Deleted: transient

Deleted: , we address this issue through a detrending of model results described later.

Deleted: (~111 km)

and historic data (Ziese et al., 2020). The previous data was augmented with daily precipitation weather station data from 01/02/2020 to 28/02/2020 obtained from Übernickel et al., (2020). We do this to include all the seasons between 2000 to 2019, i.e., from the austral autumn of 2000 to the austral summer of 2019. The periods (months of a year) of specific seasons in the Chilean Coastal Cordillera are given in Table 1. Seasonal precipitation rates were calculated by summing daily precipitation rates at three-month intervals. The seasonality and intensity of precipitation in the wet season (winter) increases from the arid (Pan de Azúcar) to humid temperate (Nahuelbuta) region.

Table 1. Months of a year corresponding to specific seasons in the Chilean Coastal Cordillera

Seasons	Months
Summer^{d*}	December - February
Autumn^{w*}	March - May
Winter^{w*}	June - August
Spring^{d*}	September - November

*d: dry season, w: wet season

NDVI derived from remote sensing imagery has been proven as an effective tool to estimate seasonal changes in vegetation cover density (Garatuza-Payán et al., 2005). Normalized difference vegetation index (NDVI) values were obtained from MODIS (Didan, Kamel, 2015) satellite data and were used as a proxy for changes in vegetation cover in the catchments. However, the major limitation of the conversion of NDVI to vegetation cover includes a saturation problem in NDVI values that occurs in high biomass regions such as our humid-temperate setting (Huete et al., 2002). This saturation can occur if the ground is covered by shrubs, at which point the information on different plant communities for associated erosion-relevant properties is lost (e.g., rooting depth, etc.). The NDVI data were acquired for 20 years (01/03/2000 – 28/02/2020), with a spatial resolution of 250 m and temporal resolution of 16 days. For application within the model simulations, the vegetation cover dataset was resampled using the nearest neighbour method to match the spatial resolution (90 m) of SRTM DEM and temporal resolution of 3 months. To summarize, season variations in precipitation rate and vegetation cover were applied to the simulations between 01/03/2000 and 28/02/2020 and encompass a 20-year record of observation variations in these factors. Additional aspects of the catchment hydrologic cycle were determined using the following approaches for the same time period previously mentioned. First, evapotranspiration (ET) data was obtained from Global Land Data Assimilation System (GLDAS) Noah version 2.1, with a monthly temporal resolution and spatial resolution of 0.25° (~28 km) (Beaudoing et al., 2020; Rodell et al., 2004). The data was obtained from March-2000 to February-2020. Due to the coarse resolution of the dataset, ET is assumed to be uniform over the entire catchment area. No higher resolution datasets were available over the 20-year time-period of interest.

Soil properties such as the grain size distribution (sand, silt, and clay fraction) and bulk density were adapted from Bernhard et al., (2018) to estimate soil water infiltration capacity in each study area. Based on these soil properties, the soils have been classified as a sandy loam (in Pan de Azúcar, Santa Gracia, and La Campana) and sandy clay loam (Nahuelbuta). Average bulk density values of 1300 kg m^{-3}, 1500 kg m^{-3}, 1300 kg m^{-3}, and 800 kg m^{-3} were used for Pan de Azúcar, Santa Gracia, La Campana, and Nahuelbuta, respectively (Bernhard et al., (2018).

Deleted: Austral Autumn

Deleted: Austral Summer

Deleted: illustrated

Deleted: up

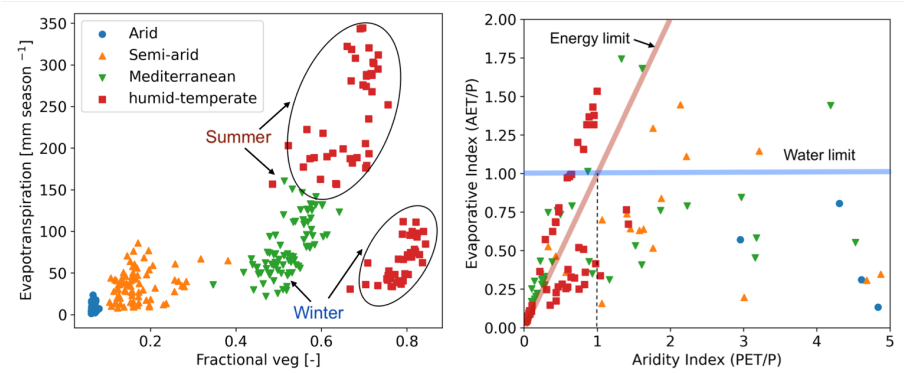

Figure 2. Parameter correlation for observations used as model input data (i.e., seasonal precipitation, vegetation cover and evapotranspiration) including: (a) fractional vegetation cover (derived from NDVI) and evapotranspiration (derived from GLDAS NOAH), (b) Budyko curve representing the relationship between precipitation (P), potential evapotranspiration (PET) and actual transpiration (AET). The points above the water limit (blue line) indicate the contribution of soil moisture to ET. The seasons (points) above the energy limit (red line) indicate the precipitation loss by infiltration. The plots represent observations corresponding to Autumn of 2000 to Summer of 2019. Each data point represents one season and are color coded by climate of the study areas. See section 3.1 for a description of the data sets used.

Figure 2 shows correlations between the model input data, such as variable climatic or hydrologic cycle metrics (i.e., precipitation and evapotranspiration) and vegetation cover for the climate of each study area investigated. The relationships shown for each area in different climate-ecological zones are based on the 20 years of data used (i.e., Autumn of 2000 – Summer of 2019). The relationship between fractional vegetation cover (V) and evapotranspiration (ET) indicates a slightly positive trend in the semi-arid setting (Fig. 2a). Whereas, the relationship in the Mediterranean setting is a steep positive gradient, with low vegetation cover (0.4– 0.55) and evapotranspiration (i.e., 50 – 100 mm season^{-1}) in the winter, which increases in summer (90 – 160 mm season^{-1}) in response to vegetation growth (i.e., V = 0.55 – 0.65). Similar trends in V and ET is indicated in the humid temperate setting during the summer with V in the range of 0.55 – 0.75 and ET ranging between 150 – 350 mm season^{-1}. However, during winters, even after high V in humid setting, lower values in ET are reported, with a positive trend. To help understand the datasets of precipitation (P) with ET, a Budyko curve is presented in figure 2b, where the actual ET (AET) and potential ET (PET) are normalized by P. In figure 2b most the data points from the humid temperate setting are above the energy limit and indicate high soil water infiltration during summer seasons. Also, data points above the water limit (blue line in Fig. 2b) indicate a carry-over in soil moisture from a wet season to few dry seasons in the humid, Mediterranean and semi-arid settings.

3.2 Estimation of runoff rates

The precipitation rates [m season^{-1}] are subjected to soil-water infiltration [m season^{-1}] and evapotranspiration [m season^{-1}] to estimate the seasonal runoff rates [mm season^{-1}]. The runoff rates (R) at every time step (t) are calculated using the actual soil-water infiltration (I_a) and the actual evapotranspiration (ET) as follows,

$$R(t) = P(t) - I_a(t) - ET(t), \quad (1)$$

Deleted:

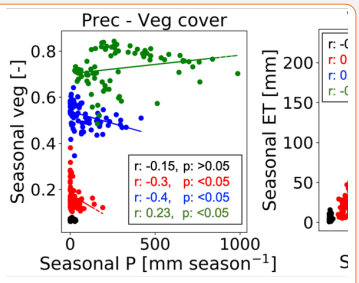

Deleted: seasonal precipitation [mm season^{-1}] and fraction of vegetation cover [-], (b) fractional seasonal vegetation cover [-] and evapotranspiration [mm], and (c) seasonal precipitation [mm season^{-1}] and evapotranspiration [mm].

Deleted: study area (AZ: Pan de Azúcar, SG: Santa Gracia, LC: La Campana, and NA: Nahuelbuta).

Deleted: Figure 2 shows correlations between the model input data, such as variable climatic or hydrologic cycle metrics (i.e., precipitation and evapotranspiration) and vegetation cover for each study area investigated. The relationships, and regression lines, shown for each area in different climate-ecological zones the general seasonal relationships over the 20 years (i.e., Autumn of 2000 – Summer of 2019) of data. For example, the correlation between seasonal precipitation and vegetation cover (Fig. 2a) illustrates a moderate negative correlation (r > -0.4) in the semi-arid (SG) and Mediterranean (LC) regions. In contrast, vegetation in the humid temperate region (NA) is positively correlated (r: 0.23). ET and vegetation cover are positively correlated (Fig. 2b) in the semi-arid (SG) and Mediterranean regions (LC). However, the correlations are negative in the humid-temperate region (NA). The correlation between seasonal precipitation and ET (Fig. 2c) is slightly positive (r: ~0.2) in the semi-arid region (SG) and moderately negative (r: -0.4) in the Mediterranean (LC) study area. However, we observe a strong negative correlation (r: -0.8) between precipitation and ET in humid-temperate and Mediterranean regions (LC and NA, Fig. 2c). This negative correlation is owed to the steep negative gradient in temperature (e.g., ~2.5 °C in NA) and solar radiation (Übernickel et al., 2020) during winters (wet season) in southern latitudes (LC and NA).¶

where, *P* is the precipitation amount in a season. This relationship was applied in the model grid cells with non-zero sediment thickness. As ET is the input parameter, there may be instances of higher ET than P in the summer seasons in the humid, Mediterranean and semi-arid settings. This is evident in figure 2b where the minimum of both values is used as ET in the given time-step.

The soil-water infiltration rate was estimated by applying the Green-Ampt equation (Green and Ampt, 1911; Julien et al., 1995):

$$f(t) = K_e\left(1 + \frac{\psi \cdot \Delta\theta}{F}\right), \quad (2)$$

where f(t) is the infiltration rate [m s^{-1}] at time t, K_e is the effective hydraulic conductivity [m s^{-1}], F is the cumulative infiltration [m], Ψ is the suction at the wetting front [m], and Δθ is the difference between saturated and initial volumetric moisture content [m^3 m^{-3}]. Effective hydraulic conductivity is highly variable and anisotropic; hence, it was considered to be uniform with a value of 1×10^{-6} m s^{-1} for each catchment.

Following the approach of Istanbulluoglu and Bras, (2006) for loamy soils, the soil-water infiltration was modified to account for variable vegetation cover in each grid cell, as follows:

$$I_c(t) = f(t)(1 - V(t)) + 4f(t)(V(t)), \quad (3)$$

$$I_a(t) = Min[P(t), I_c(t)], \quad (4)$$

where I_c is the infiltration capacity and V is the vegetation cover (between 0 and 1) in a model grid cell at time-step *t*. Values used in the simulations for the parameters in equations 2-4 are provided in appendix Table A1.

3.3 Model setup

We applied the Landlab landscape evolution model, a python-based modeling toolkit (Hobley et al., 2017), combined with the SPACE 1.0 model (Shobe et al., 2017). The SPACE model allows coupled detachment-transport limited fluvial processes with simultaneous bedrock erosion and sediment entrainment/deposition. The Landlab-SPACE programs were applied using a set of runtime scripts and input files (Sharma and Ehlers, 2023) to account for vegetation and climate change effects on catchment erosion (i.e., fluvial erosion and hillslope diffusion), using the approach described in Schmid et al. (2018) and Sharma et al. (2021). In addition, the geomorphic processes considered involve weathering and regolith production (Barnhart et al., 2019) and infiltration of surface water into soil (Rengers et al., 2016) based on the Green-Ampt method (Green and Ampt, 1911), and runoff modeling.

The model parameters (Table. A1) are selected for the distinct climate and ecological settings in the Chilean Coastal Cordillera based on the observations presented in Schaller et al., (2018). The model state parameters (i.e., erodibility, diffusivity, rock uplift rate, etc.) in the simulations are adapted from Sharma et al., (2021). The model was simulated at a seasonal scale (time step of three months) from the autumn of 2000 (01/03/2000) to the summer of 2019 (28/02/2020). Simulations were conducted for a total time of 1000 years with a time-step of 1 season (3 months) with 20 years (2000 – 2019) of observations in vegetation and precipitation. These 20-years of observations were repeated (looped) 50 times, to identify, and detrend, long-term transient trends in catchment erosion rates due to potential differences in actual and assumed erosional parameters such as the hillslope diffusivity or fluvial erodibility. The combined effects of temporally variable (at seasonal scale) precipitation and vegetation cover (also spatially variable) on catchment-scale erosion rates are therefore the primary factors influencing predicted erosion rates.

Deleted: module of Shobe at al. (2017). The SPACE module

Deleted: modified for vegetation-dependent hillslope processes (Johnstone and Hilley, 2014) and vegetation-dependent overland flow and fluvial erosion using the approach described in Schmid et al.

Deleted: calibrated to

Deleted: of

Deleted: erosion, diffusion, lithology, tectonic

Deleted: Autumn

Deleted: Summer

Deleted: effect

Deleted: was

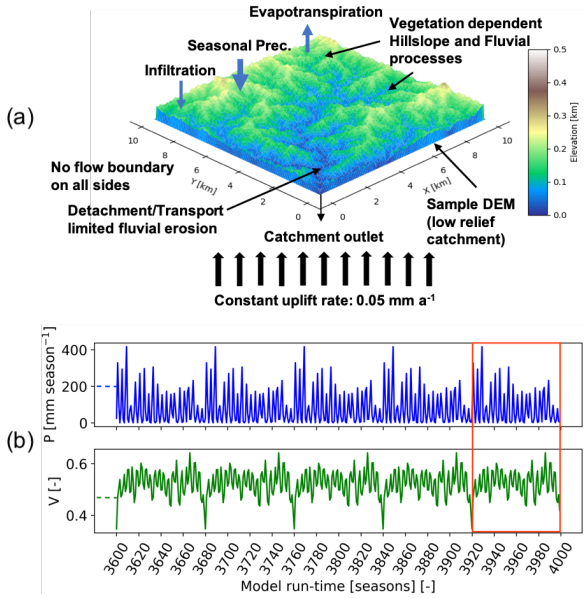

Figure 3. Schematic of the model geometry and seasonal precipitation and vegetation forcings used in this study. (a) Model setup representing sample DEM (low relief catchment) with no flow boundaries on all sides and a single catchment outlet. The model involves vegetation-dependent seasonal hillslope and fluvial processes and rainfall-infiltration-runoff modeling. (b) Seasonal precipitation and vegetation cover dataset (Mediterranean, La Campana, setting) for the last five iterations of model simulations. The results of highlighted iterations (after detrending for long-term transients) are analyzed in consecutive sections.

3.4 Boundary and initial conditions

The boundaries are closed (no flow) on all sides, with a single stream outlet at the point of minimum elevation at boundary nodes (Fig. 3). Initial sediment cover thickness is considered uniform across the model domain, and was approximated based on observations by Schaller et al., (2018) and Dal Bo et al., (2019). The sediment thickness used are 0.2 m in the arid (AZ), 0.45 m in semi-arid (SG), 0.6 m in the Mediterranean (LC), and 0.7 m in humid temperate (NA) catchments. The rock uplift rate is kept constant throughout the entire model run as 0.05 mm yr^{-1}, adapted from a similar study (Sharma et al., 2021).

Deleted: initial

3.5 Overview of simulations conducted

The simulations were designed to identify the sensitivity of erosion rates to seasonal variations in either precipitation rates or vegetation cover, as well as the more realistic scenario of coupled seasonal variations in both vegetation cover and precipitation. We evaluated this sensitivity with a step-wise increase in model complexity. Three sets of simulations were designed for the four selected study areas, which are as follows,

1. Scenario 1: Influence of constant (mean seasonal) precipitation with seasonal variations in vegetation cover catchment-scale erosion rates.

2. Scenario 2: Influence of seasonal variation in precipitation and constant (mean seasonal) vegetation cover on catchment-scale erosion rates.
3. Scenario 3: Influence of coupled seasonal variations in both precipitation and vegetation cover on catchment-scale erosion rates.

The results for scenarios 1 – 3 are illustrated in sections 4.1, 4.2, and 4.3, respectively.

3.6 Detrending of results for long term transients

Model simulations were conducted for 1,000 years using 20 years [March-2000 – Feb-2020] of observations in vegetation cover, and precipitation and were repeated 50 times for a total simulation duration of 1000 years. Simulations presented here were conducted on the present-day topography to allow for the application of observed time series of precipitation and vegetation change in different ecosystems and study areas. This choice of setting comes with the compromise that the erosional parameters (e.g., diffusivity, erodibility, etc.) used in the model are likely not the same as those that led to the present-day catchment topography. As a result, a long-term transient in erosion rates is expected as the model tries to reach an equilibrium with assumed erosional parameters. To correct for any long-term transients in erosion influencing our interpretations, we conducted a linear detrending of the results to remove any long-term variations. The detrending was conducted through a linear regression over entire time series of 1000 years and the values were corrected using the slope of the regression line. Hence, the detrended model results for the last 20 years were analyzed and discussed in sections 4 and 5. In practice, the detrending of time series did not impart a significant change to the results presented.

4 Results

In the following sections, we focus our analysis on the mean catchment erosion rates over seasonal (3 months) time scales (see Table. 1). In all scenarios, the rock uplift rate was kept constant at 0.05 mm yr^{-1} following the approach of Sharma et al. (2021). For simple representation, the results of the last five years of the last cycle of transient simulations starting from Autumn-2015 to Summer-2019 are displayed in Fig. 4, 6, and 8 (after detrending, see section 3.6). The results for the entire time series (Autumn-2000 – Summer-2019) are available in the supplement (Fig. 1 – 3). The precipitation and erosion rates are shown with the units [mm $season^{-1}$].

4.1 Scenario 1: Influence of constant precipitation and seasonal variations in vegetation cover on erosion rates

In scenario 1, vegetation cover (MODIS NDVI from March 2000 to February 2020) fluctuates seasonally (Fig. 4b), and precipitation rates are kept constant at the seasonal mean (i.e., MAP divided by the number of seasons in a year) during the entire time-series (Fig. 4a) (Ziese et al., 2020). The range of seasonal vegetation cover variations (and mean seasonal precipitation rates) are observed as 0.06 – 0.08 (3.92 mm $season^{-1}$), 0.1 – 0.4 (20.16 mm $season^{-1}$), 0.35 – 0.65 (79 mm $season^{-1}$), and 0.5 – 0.85 (292 mm $season^{-1}$) for the arid, semi-arid, Mediterranean and, humid temperate settings, respectively (Figs. 4a-b). The predicted mean catchment seasonal erosion rates range between $0 - 6 \times 10^{-4}$ mm $season^{-1}$, $0 - 9.4 \times 10^{-4}$ mm $season^{-1}$, $0 - 2.3 \times 10^{-3}$ mm $season^{-1}$, and $1.2 \times 10^{-3} - 4 \times 10^{-3}$ mm $season^{-1}$ for the arid, semi-arid, Mediterranean and humid temperate settings, respectively (Fig. 4c).

To analyze the relationships between the relative changes in forcings and responses, seasonal changes in vegetation cover and erosion rates were normalized between 0 and 1 and plotted in Figs. 5a-d. An inverse relationship and negative correlation (Kendall-tau correlation coefficient: 0.4 – 0.5) is visible between the normalized catchment erosion rates and vegetation cover for the dry season and wet season separately in the humid temperate (Fig. 5d) and Mediterranean settings (Fig. 5c). The linear relationship in vegetation and erosion change in the Mediterranean and humid-temperate settings indicates that these

Moved (insertion) [1]

Deleted: 4a) (Ziese et al., 2020). The range of seasonal vegetation cover variations (and mean seasonal precipitation rates) are observed as 0.06 – 0.08 [-] (3.92 mm $season^{-1}$), 0.1 – 0.4 [-] (20.16 mm $season^{-1}$), 0.35 – 0.65 [-] (79 mm $season^{-1}$), and 0.5 – 0.85 [-] (292 mm $season^{-1}$) for the Pan de Azúcar, Santa Gracia, La Campana and Nahuelbuta study areas (Fig. 1), respectively.

Deleted: The predicted mean catchment

Deleted: range between $0 - 6 \times 10^{-4}$ mm $season^{-1}$, $0 - 9.4 \times 10^{-4}$ mm $season^{-1}$, $0 - 2.3 \times 10^{-3}$ mm $season^{-1}$, and $1.2 \times 10^{-3} - 4 \times 10^{-3}$ mm $season^{-1}$ in Pan de Azúcar, Santa Gracia, La Campana, and Nahuelbuta, respectively (Fig.

Moved up [1]: 4c).

Deleted: The mean catchment seasonal

Deleted: have an inverse linear relationship with seasonal

Deleted: arid, semi-arid,

Deleted: 5). However, this relationship is positive in the humid-temperate setting, i.e., erosion increases with an increase in vegetation cover with a relatively lower gradient (3×10^{-3}).¶
The maximum gradient between

Deleted: cover

Deleted: rates is observed

Deleted: region (La Campana, gradient: -6×10^{-3}). The slopes in the vegetation cover – erosion rate relationship (Fig. 5) represent the sensitivity of each catchment to changes in seasonal vegetation cover, which

Deleted: the Mediterranean region (La Campana) is ~4.5 times more sensitive than the semi-arid region (Santa Gracia). Due to very low precipitation in the arid region (Pan de Azúcar), no significant range in erosion rates is observed (e.g., Pearson r: 0.17; p: >0.05). The results (Fig. 4 and 5) suggest a high sensitivity in erosion in the Mediterranean setting to changes in seasonal vegetation cover (i.e., erosion rates decrease with an increase in vegetation cover). The erosion rates are low (e.g., <0.005 mm season-1) due to low mean precipitation rates subjected to infiltration and evapotranspiration

catchments are dominated by fluvial (water driven) and overland flow processes, and the role of hillslope diffusion is minimal. In contrast, no correlation was found for the arid and semi-arid settings.

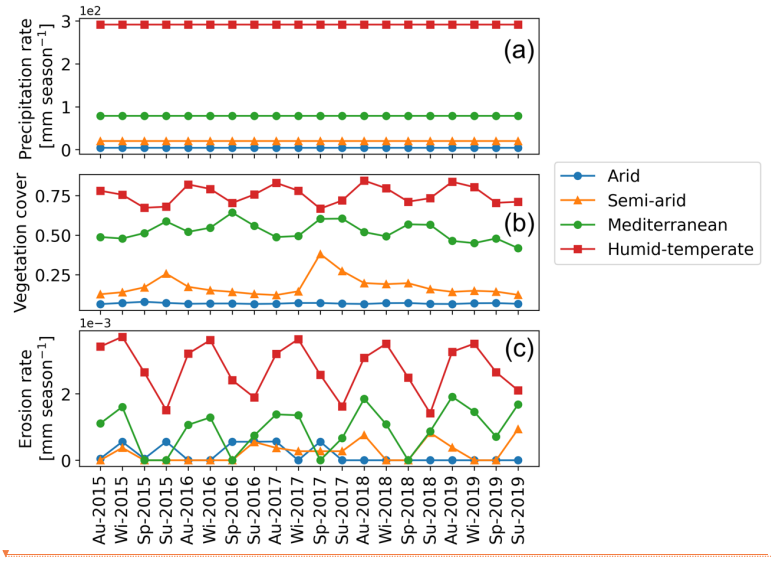

Figure 4. Results of simulations with constant seasonal precipitation and variable vegetation over last 5 years (Autumn-2015 – Summer-2019) of last cycle of transient-state model run representing: (a) mean catchment seasonal precipitation rates [mm season^{-1}], (b) mean catchment seasonal vegetation cover [-], and (c) mean catchment seasonal erosion rates [mm season^{-1}].

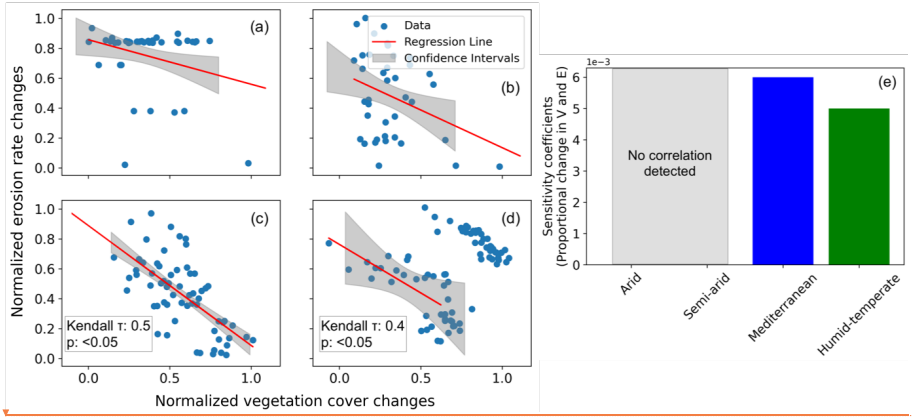

Figure 5. Seasonal changes (normalized) in vegetation cover and erosion rates for the scenario with constant precipitation and seasonal changes in vegetation cover in (a) arid, (b) semi-arid, (c) Mediterranean, and (d) humid-temperate settings, with the information on confidence interval (grey shading) and Kendall-tau correlation coefficients.

Formatted: Font: Not Bold

Deleted:

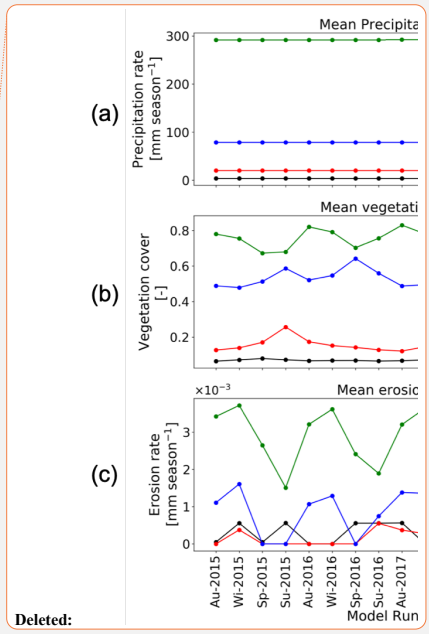

Deleted:

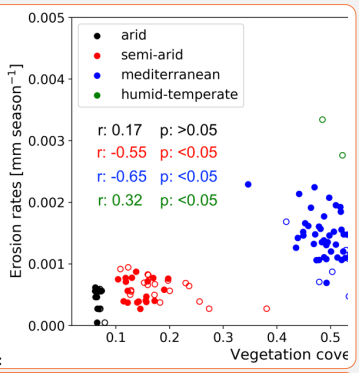

Deleted: Correlation of

Deleted: [-]

Deleted: [mm season^{-1}] obtained from simulations

Deleted: seasonal

Deleted: variable

Deleted: over the last cycle

(e) Sensitivity coefficients for proportional changes in vegetation cover and erosion rates based on the slope and intercept of the regression lines for the above environmental settings. The sensitivity coefficient is defined as the slope of the regression line presented in sub-sections a-d.

The sensitivity coefficients based on slope and intercept of the regression lines (Figs. 5a-d) are plotted in Fig. 5e. The results indicate a higher sensitivity of erosion rates to seasonal vegetation changes in the Mediterranean setting relative to humid-temperate setting. However, in the arid and semi-arid settings, the lack of a significant correlation in the change in vegetation cover and erosion rates leads to a low sensitivity. This is owed to very low mean precipitation rates (<20 mm season^{-1}) in the arid and semi-arid settings. The predicted erosion rates are relatively low (e.g., <0.004 mm season^{-1}) in this scenario, due to low mean precipitation rates, which are primarily subjected to infiltration and evapotranspiration in these drier settings.

4.2 Scenario 2: Influence of seasonal variations in precipitation and constant vegetation cover on erosion rates

In scenario 2, vegetation cover (MODIS NDVI from Mar-2000 – Feb-2020) is kept constant at the mean seasonal vegetation cover (Fig. 6b) and precipitation rates vary seasonally (Mar-2000 – Feb-2020) (Fig. 6a). The range of seasonal precipitation rate variations are observed in the range of 0 – 32.42 mm season^{-1}, 0 – 191.66 mm season^{-1}, 0.03 – 417 mm season^{-1}, and 26 – 987 mm season^{-1} in the arid, semi-arid, Mediterranean and, humid temperate settings, respectively.

The simulated mean catchment seasonal erosion rates are observed in the range of $0 - 2 \times 10^{-3}$ mm season^{-1}, $0 - 8.3 \times 10^{-3}$ mm season^{-1}, $0 - 1.37 \times 10^{-2}$ mm season^{-1}, and $0 - 1.3 \times 10^{-2}$ mm season^{-1} in the arid, semi-arid, Mediterranean and, humid temperate settings, respectively (Fig. 6c).

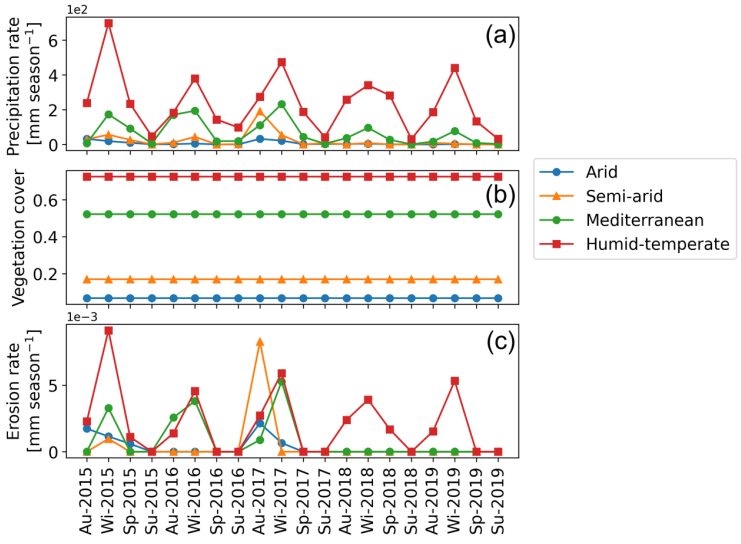

Figure 6. Results of simulations with variable seasonal precipitation and constant vegetation over last 5 years (Autumn-2015 – Summer-2019) of last cycle of transient-state model run representing: (a) mean catchment seasonal precipitation rates [mm season^{-1}], (b) mean catchment seasonal vegetation cover [-], and (c) mean catchment seasonal erosion rates [mm season^{-1}].

Deleted: transient state model run (Autumn-2000 – Summer-2019). Hollow circles: dry season; filled circles: wet season. Each individual circle represents one

Formatted: Space After: 0 pt

Deleted: season within the timeseries

Formatted: Font: Not Bold

Formatted: Font: Not Bold, Not Italic

Formatted: Font: Not Bold

Deleted: for Pan de Azúcar, Santa Gracia, La Campana and Nahuelbuta

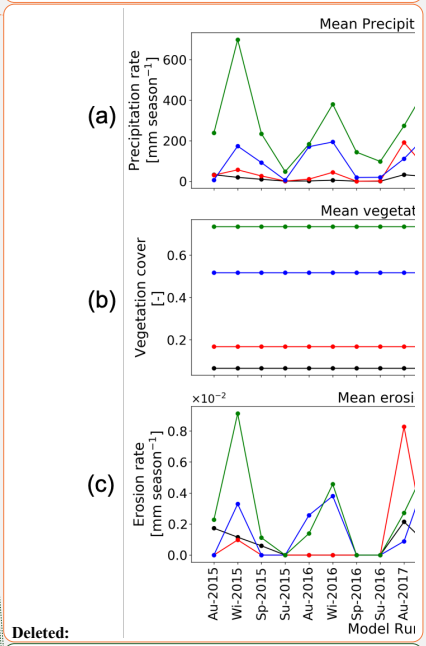

Deleted:

Moved (insertion) [2]

Moved (insertion) [3]

Similar to scenario 1, the changes in seasonal precipitation and erosion rates were normalized between 0 and 1 and plotted in Figs. 7a-d. A strong positive correlation (Kendall-tau correlation coefficient ranging from 0.5 in semi-arid to 0.9 in Mediterranean and humid-temperate settings) in the normalized precipitation and erosion rates changes is predicted with the majority of the data points within the 95% confidence interval in all the settings. The sensitivity coefficients based on the proportional changes in precipitation and erosion rates, indicate the highest sensitivity in semi-arid settings) with ~5%, ~11% and ~67% lower sensitivities in the arid, Mediterranean, and humid-temperate settings, respectively (Fig. 7e). This may be owed to the occasional El Niño events with extremely high precipitation occurring in the arid and semi-arid settings (with sparse vegetation cover).

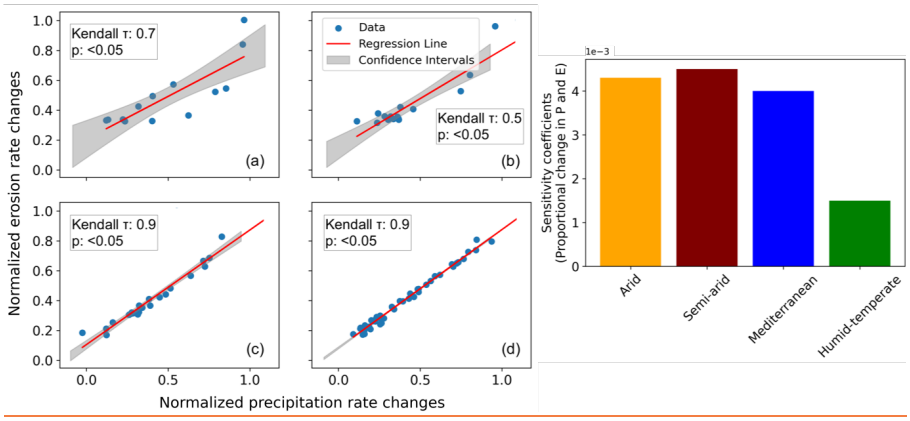

Figure 7. Seasonal changes (normalized) in precipitation and erosion rates for the scenario with seasonal changes in precipitation rates and constant vegetation cover in (a) arid, (b) semi-arid, (c) Mediterranean, and (d) humid-temperate settings, with the information on confidence interval (grey shading) and Kendall-tau correlation coefficients. (e) Sensitivity coefficients for proportional changes in precipitation and erosion rates based on the slope and intercept of the regression lines for the above environmental settings. The sensitivity coefficient is defined as the slope of the regression line presented in sub-sections a-d.

4.3 Scenario 3: Influence of coupled seasonal variations in both precipitation and vegetation cover on erosion rates

In this scenario, coupled variations in seasonal vegetation cover (MODIS NDVI from Mar-2000 – Feb-2020) (Fig. 8b) and precipitation rates are presented for the years 2000 - 2019 (Fig. 8a). The range of seasonal precipitation rates (and seasonal vegetation cover, V) variations are 0 – 32.42 mm season^{-1} (V= 0.06 – 0.08), 0 – 191.66 mm season^{-1} (0.1 – 0.38), 0.03 – 417 mm season^{-1} (0.35 – 0.65), and 26 – 987 mm season^{-1} (0.5 – 0.85) in the arid, semi-arid, Mediterranean and humid temperate settings, respectively (Figs. 8a-b). The mean catchment seasonal erosion rates range between $0 - 2 \times 10^{-3}$ mm season^{-1}, $0 - 1 \times 10^{-2}$ mm season^{-1}, $0 - 1.4 \times 10^{-2}$ mm season^{-1}, and $0 - 1.4 \times 10^{-2}$ mm season^{-1} in the arid, semi-arid, Mediterranean and, humid temperate settings, respectively (Fig. 8c).

Changes in precipitation on erosion rates were normalized between 0 and 1 and plotted in figures. 9a-d. Similar to the results from scenario 2, a strong positive correlation was predicted in all the environmental settings. The sensitivity coefficients based on the proportional changes in precipitation and erosion rates, indicate the highest sensitivity in the semi-arid settings with ~25% and ~71% lower sensitivities in arid and Mediterranean, and humid-temperate settings, respectively (Fig. 9e). Similarly, the isolated effect of changes the in the vegetation cover on erosion rates (Fig. 10) does not yield a significant correlation in

Moved up [2]: The simulated mean catchment seasonal erosion rates are observed in the range of $0 - 2 \times 10^{-3}$ mm season^{-1}, $0 - 8.3 \times 10^{-3}$ mm season^{-1}, $0 - 1.37 \times 10^{-2}$ mm season^{-1}, and $0 - 1.3 \times 10^{-2}$ mm season^{-1} in

Moved up [3]: 6c).

Deleted: Pan de Azúcar, Santa Gracia, La Campana, and Nahuelbuta, respectively (Fig.

Deleted: The mean catchment seasonal erosion rates are positively correlated with seasonal precipitation rates (Fig. 7), with a maximum gradient in the arid region (AZ, gradient: ~1.3×10^{-4}).¶
The gradients in the precipitation – erosion rate relationship (Fig. 7) indicate the sensitivity of each catchment

Deleted: rates, such that that the arid region (AZ) is ~2.7, ~3.2,

Deleted: ~8 times more sensitive than

Deleted: (SG),

Deleted: (LC)

Deleted: region (NA), respectively. The results (Fig. 6

Deleted: 7) suggest a high sensitivity of erosion

Moved (insertion) [4]

Deleted: to changes in seasonal precipitation rates (i.e., erosion increases at relatively higher rates with an increase

Formatted: Font: Bold

Deleted:). The erosion rates are higher than in scenario 1 (e.g., 0 – 0.014 mm season^{-1}) due to higher precipitation rates ... [1]

Deleted: 2.¶ ... [2]

Formatted: Font: Bold

Moved up [4]: Figure 7.

Formatted ... [3]

Deleted: Correlation of precipitation rates [mm season^{-1}] ... [4]

Deleted: [-]),

Deleted: [-]),

Deleted: [-]),

Deleted: [-]) for Pan de Azúcar, Santa Gracia, La Campana

Deleted: Nahuelbuta

Moved (insertion) [5]

Deleted: .

Deleted: The mean catchment seasonal erosion rates are ... [5]

Deleted: the range of $0 - 2 \times 10^{-3}$ mm season^{-1}, 0 – ... [6]

Moved up [5]: 8c).

Deleted: Similar to scenario 2, mean catchment seasonal ... [7]

Deleted: rates (Fig. 9), with a maximum gradient in an arid ... [8]

Deleted: – erosion rate relationship (Fig. 9) represent the ... [9]

Deleted: vegetation cover. The results (Fig. 8 and 9)

Deleted: that

Deleted: arid region (AZ) is ~2.3, ~3, and ~8 times more ... [10]

Deleted: (SG),

Deleted: (LC),

Deleted: region (NA), respectively.

arid, semi-arid and Mediterranean settings. However, we observe a strong negative correlation in the humid-temperate setting (Fig. 10d) during the wet season (Kendall tau correlation coefficient: -0.6, with >95% significance level). Hence, the sensitivity coefficients in this case are not plotted.

The similarity in results obtained from scenarios 2 and 3 suggest a first-order control of seasonal precipitation changes on erosion rates (~70% higher sensitivity to changes in precipitation), with less significance to vegetation cover changes. For example, the sensitivity of erosion to precipitation rate changes in semi-arid setting is predicted as ~70% higher to that of humid-temperate setting in both the scenarios.

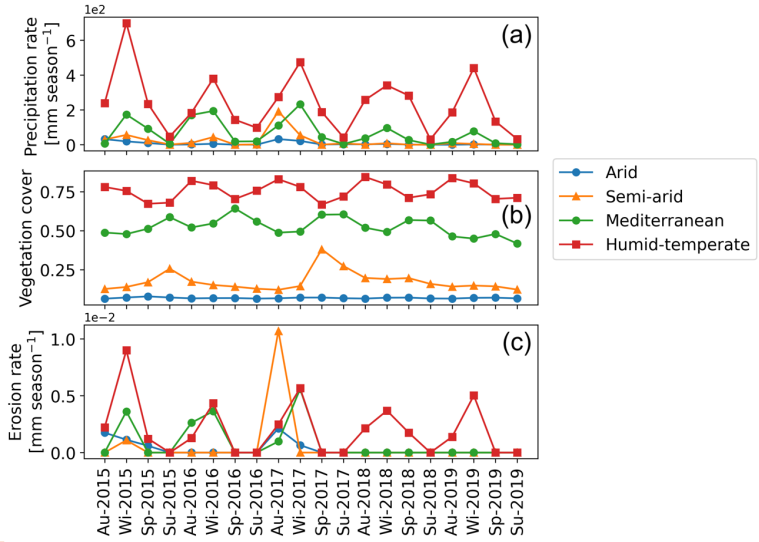

Figure 8. Results of simulations with coupled variations in seasonal precipitation and vegetation over the last five years (Autumn-2015 – Summer-2019) of the last cycle of transient-state model run representing: (a) mean catchment seasonal precipitation rates [mm season^{-1}], (b) mean catchment seasonal vegetation cover [-], and (c) mean catchment seasonal erosion rates [mm season^{-1}].

Deleted: the

Deleted: (e.g., Pearson r > 0.6 for arid setting, Fig. 9a

Deleted: changing

Deleted: (Pearson r < -0.19 for

Deleted: , Fig. 9b).

Deleted:

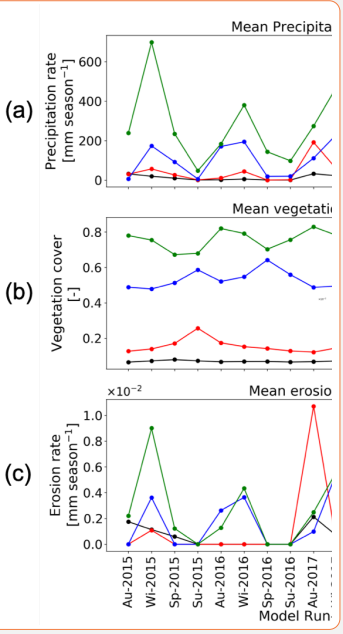

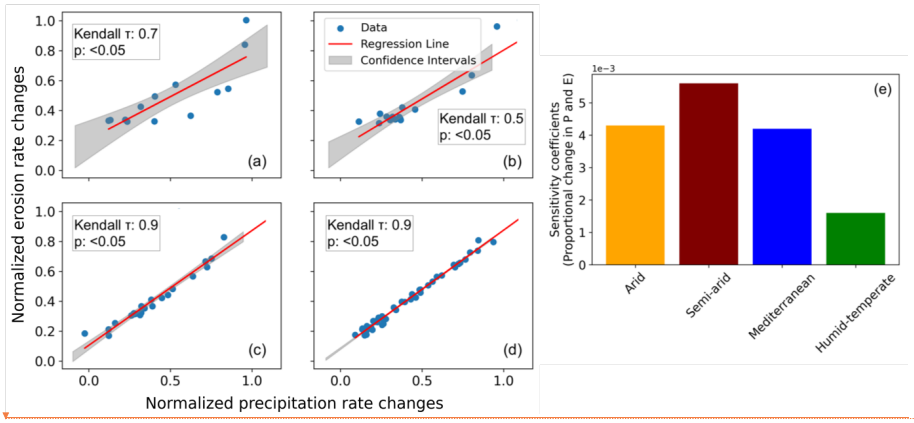

Figure 9. Seasonal changes (normalized) in precipitation and erosion rates for the scenario with coupled seasonal changes in both precipitation rates and vegetation cover in (a) arid, (b) semi-arid, (c) Mediterranean, and (d) humid-temperate settings, with the information on confidence interval (grey shading) and Kendall-tau correlation coefficients. (e) Sensitivity coefficients for proportional changes in precipitation and erosion rates based on the slope and intercept of the regression lines for the above environmental settings. The sensitivity coefficient is defined as the slope of the regression line presented in sub-sections a-d.

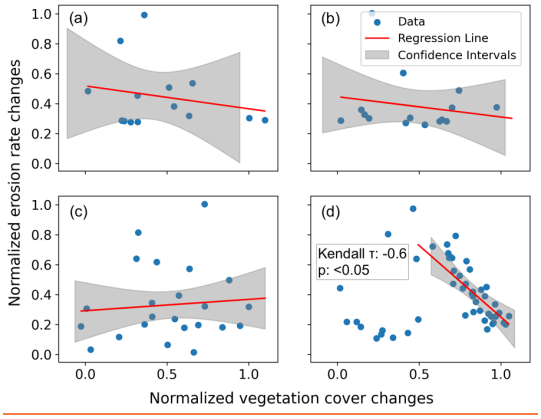

Figure 10. Seasonal changes (normalized) in vegetation cover and erosion rates for the scenario with coupled seasonal changes in both precipitation rates and vegetation cover in (a) arid, (b) semi-arid, (c) Mediterranean, and (d) humid-temperate settings, with the information on confidence interval (grey shading) and Kendall-tau correlation coefficients.

Deleted:

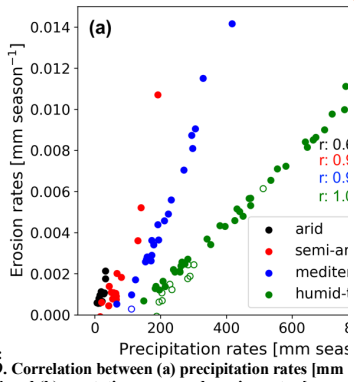

Figure 9. Correlation between (a) precipitation rates [mm season^{-1}] and (b) vegetation cover and erosion rates [mm season^{-1}] obtained from simulations with coupled variations in seasonal precipitation and vegetation over the last cycle of the transient simulation (Autumn-2000 – Summer-2019). Hollow circles: dry season; filled circles: wet season. Each individual circle represents one predicted season within the timeseries.¶

¶

5 Discussion

This section discusses the relationship between variations in seasonal precipitation and vegetation cover with erosion rates in the form of the amplitude of change for each model scenario (section 5.1). This is followed by the synthesis of catchment scale erosion rates variability over wet and dry seasons (section 5.2). In section 5.3, we discuss the impact transient dynamics of sediment transport in our modelling approach. Finally, we compare our results with previously published studies (section 5.4) and discuss model limitations (section 5.5).

5.1 Synthesis of the amplitude of change in erosion rates for model scenarios 1-3

The amplitude of change of mean catchment erosion rates [in percentage] varies at a seasonal scale (Fig. 11) between the study areas. The amplitude of change in erosion rates to their respective mean values was estimated (Fig. 11) using the coefficient of variation in percent (standard deviation divided by the mean of a dataset). The coefficient of variation is a statistical tool to compare multiple variables free from scale effects. It is a dimensionless quantity (Brown, 1998). This comparison represents the sensitivity of each catchment to changing seasonal weather for all three model scenarios (sections 4.1 – 4.3).

In scenario 1, with seasonal variations in vegetation cover and constant seasonal precipitation (Fig. 11), the amplitude of change in erosion rates ranges between 5% in the arid and 36% in Mediterranean setting. The above results support the findings of Zhang et al. (2019), which observed 20-30% of the total change in sediment yield with constant precipitation and variable vegetation cover. The above study used the soil and water assessment tool (SWAT) based on NDVI and climate parameters.

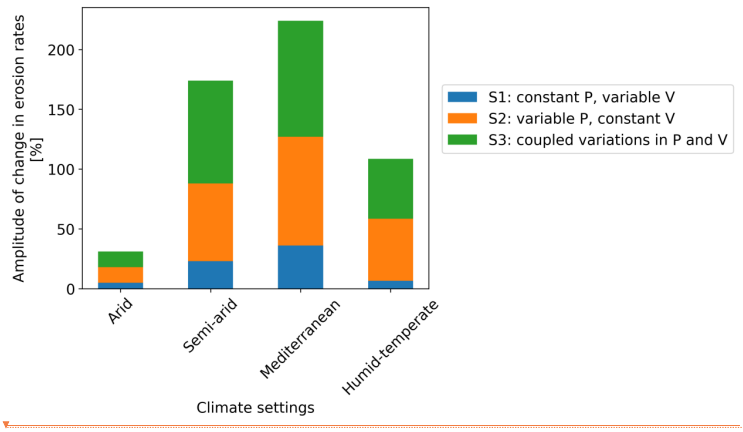

Figure 11. Stacked bar plot depicting the amplitude of change in seasonal erosion rates (relative to their respective means). Scenario 1 is shown in blue and had variable vegetation cover and constant precipitation rates. Scenario 2 is shown in orange and had constant vegetation cover and variable precipitation rates, and scenario 3 is shown in green and represents the simulation with coupled variations in vegetation cover and precipitation rates.

In scenario 2, with constant vegetation cover and variable precipitation rates (Fig. 11), the amplitude of change in erosion rates ranges from 13% in the arid setting (AZ) to 52%, 65%, and 91% in humid-temperate (NA), semi-arid (SG) and Mediterranean (LC) settings, respectively. A similar trend is observed in scenario 3 with coupled variations in vegetation cover and precipitation rates (Fig. 11), with the amplitude of change in erosion rates between 13% in the arid setting up to 50%, 86%, and 97% in the humid-temperate, semi-arid and Mediterranean settings, respectively. The magnitude of erosion rate changes is amplified in scenario 3, especially in the semi-arid setting (e.g., ~21% increase in the amplitude of change from scenario 2

Deleted: a discussion of the effect of variable vegetation and precipitation rates on seasonal erosion rates (section 5.2). Following this, we present

Deleted:).

Deleted: 10

Deleted: 10

Deleted: , i.e., it

Deleted: section

Deleted: 10a

Deleted: 6.

Deleted: humid-temperate setting

Deleted: In addition, a 5.5% change in amplitude in erosion rates is observed in the arid setting (Fig. 10a). However, due to the weak correlation between vegetation cover and erosion rates (i.e., Pearson r: 0.17 and p>0.05, Fig. 5) and negligible vegetation cover (V < 0.1), it is unclear if these changes in erosion rates are due to changes in vegetation cover alone.

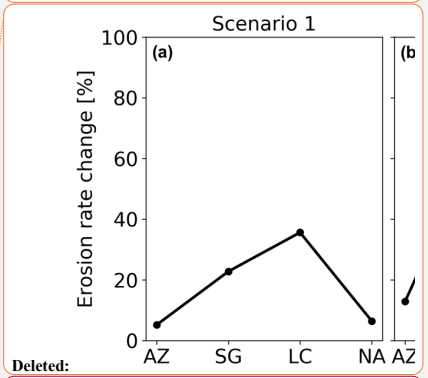

Deleted:

Deleted: 0

Deleted: The

Deleted:)

Deleted: (a) scenario 1: with

Deleted: , (b) scenario

Deleted: : with

Deleted: (c)

Deleted: :

Deleted: 10b

Deleted: 10c

to scenario 3). This amplification could be owed to the 35% change in vegetation cover in the semi-arid setting (Fig. 8). Overall, these observations indicate a high sensitivity of erosion in semi-arid and Mediterranean environments compared to arid and humid-temperate settings.

The pattern of erosion rate changes in scenarios 1-3 implies a dominant control of precipitation variations (rather than vegetation cover change) on catchment erosion rates at a seasonal scale. This interpretation is consistent with previous observational studies. For example, a field study by Suescún et al. (2017) in the Columbian Andes highlighted the significant influence of precipitation seasonality (over vegetation cover seasonality) on runoff and erosion rates. An observational catchment-scale study in the semi-arid Chinese Loess Plateau by Wei et al. (2015) indicated that intra-annual precipitation variations were a significant contributor to monthly runoff and sediment yield variations.

5.2 Synthesis of catchment erosion rates over wet and dry seasons

In this section, we discuss the ratio of seasonal precipitation and erosion rates with the mean annual precipitation (MAP) (Fig. 12a) and mean annual erosion (MAE) (Fig. 12b) during different seasons (i.e., autumn – summer) in a year, averaged over the last cycle of the transient simulations (i.e., depicting the erosion rate predictions for 2000 – 2019). These are defined as the ratio of the mean erosion (and precipitation) rates in a season (e.g., winter) to the mean annual erosion rates (and MAP) during the last 20 years of the transient simulations. This was done to identify the impact of precipitation during wet seasons (in this case, winter) in influencing the annual erosion rates. This analysis was performed for the simulation results of scenario 3 for different climate and ecological settings (i.e., arid to humid-temperate). We do this specifically with scenario 3 results to capture the trends in erosion rates with coupled variations in model input (i.e., precipitation and vegetation cover).

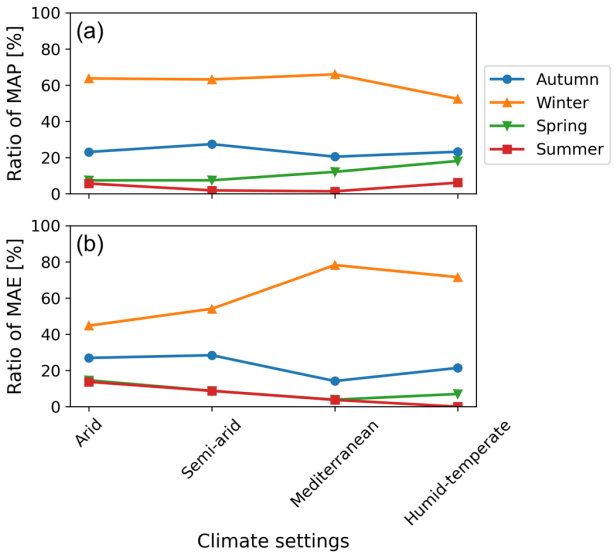

Figure 12. The ratio of seasonal precipitation and erosion rates to mean annual precipitation (MAP) and mean annual erosion (MAE) during the last cycle of transient simulations results from scenario 3 (coupled seasonal variations in precipitation and vegetation cover). The plots correspond to (a) the ratio of MAP per season [%] and (b) ratio of MAE

Deleted: predominant

Deleted: For example, a plot-scale study by Gabarrón-Galeote et al. (2013) in the Mediterranean environment in Belgium concluded that rainfall intensity was the main factor in determining the observed seasonal soil hydrological and erosive response. Another

Deleted: 11a

Deleted: 11b

Deleted: entire time series (

Deleted: is

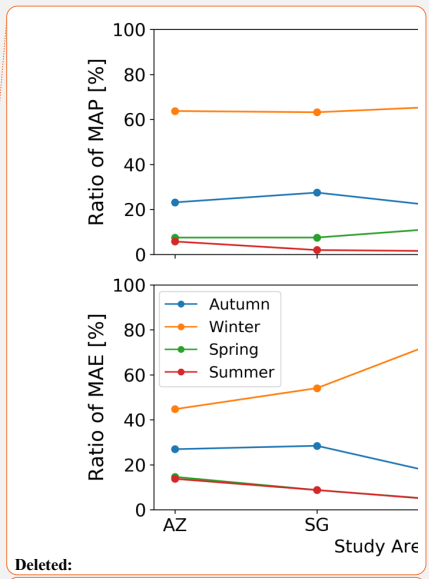

Deleted:

Deleted: 11

Deleted: model variables

Deleted: means

Deleted: all

Deleted: seasons in a year for simulation

per season [%]. Each color and point style represent the ratio for a distinct climate setting i.e., arid, semi-arid, Mediterranean, and humid-temperate settings.

The values for the ratio of MAP during different seasons (Fig. 12a) depicts winter (June-August) and summer (December-February) as the wettest and driest seasons of the year, respectively. For example, all study areas receive >50% and <6% of MAP during winters and summers. The same is reflected in Fig. 12b with 45%, 55%, 78%, and 71% of MAE in the arid, semi-arid, Mediterranean, and humid-temperate settings, respectively, during winters. On the contrary, during summers the share of MAE decreases from 14% in the arid setting to 1% in the humid-temperate setting. The Autumn (March-May) receives lower precipitation amounts that range from 20–30% of MAP in the study areas. Arid and semi-arid settings experience a relatively higher share of MAE (e.g., ~30%) than the Mediterranean and humid temperate settings (e.g., ~15-20%). The Spring season experiences relatively higher erosion rates despite a smaller share of MAP in arid and semi-arid settings. For example, the arid and semi-arid settings experience 10-14% of the MAE for ~7% of MAP. At the same time, the Mediterranean and humid-temperate settings experience 5-7% of MAE for ~12-18% of MAP during Spring. Overall, we find that arid and semi-arid settings experience <15% and ~50% of MAE during the wet (winter) and dry (summer) seasons. The above relationship is amplified for the Mediterranean and humid-temperate settings with <5% and >70% of MAE occurring during wet and dry seasons, respectively. The latter is in agreement with an observational study by Mosaffaie et al., (2015) in a Mediterranean catchment in Iran. More specifically, Mosaffaie et al., (2015) used field observations from 2012-2013 to conclude that maximum erosion rates (>70%) are observed during the wet season, which decreases in the dry season (<10%).

5.3 Consideration of transient sediment dynamics in model results

This section discusses the impact of lag times from when sediment is eroded in a source area until it leaves the catchment outlet. This analysis was conducted because in natural systems, when sediment is eroded from its source, it takes time to leave the catchment (in this case the model domain) and recorded as eroded in our analysis. According to field studies and modeling experiments, this time lag is usually more than a season (3 months) (e.g., Buendia et al., (2016)). To capture these time-lags in precipitation, erosion and concentration of sediment leaving the catchment outlet, the model output for the Mediterranean and humid-temperate settings are compared (Fig. 13). We perform this analysis on the simulation results of scenario 3 with coupled variations in seasonal precipitation and vegetation cover. The concentration of sediment is defined as a dimensionless quantity (Qs/Q) estimated from sediment flux (Qs) and discharge rates (Q).

Deleted: [%] of the mean values averaged over the last 20 years of the simulations (2000 - 2019).

Deleted: represents

Deleted: each ecological

Deleted: (Pan de Azúcar, AZ),

Deleted: (Santa Gracia, SG),

Deleted: (La Campana, LC),

Deleted: (Nahuelbuta, NA).

Deleted: 11a

Deleted: 11b

Formatted: Font color: Text 1

Deleted: 5.3

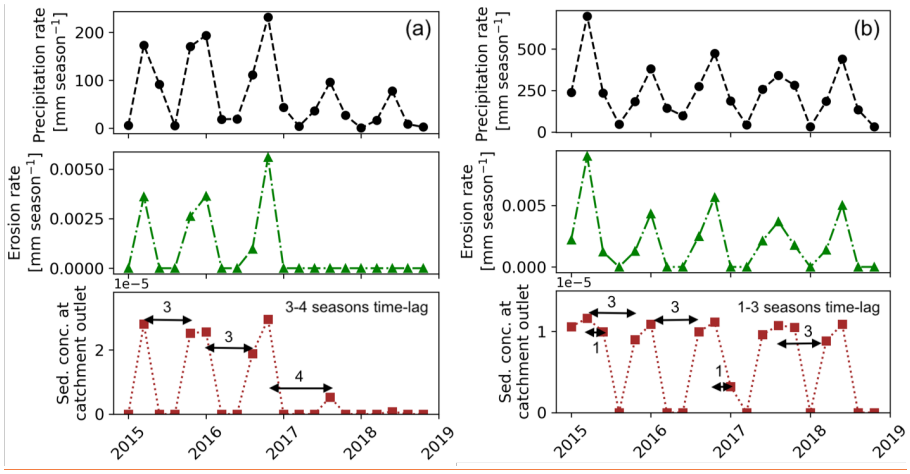

Figure 13. Simulation results (scenario 3: coupled variations in precipitation in vegetation cover) to capture the time-lags in precipitation, erosion rates and sediment concentration at catchment outlet) over the last five years (Autumn-2015 – Summer-2019) of the last cycle of transient-state model run for the catchments in: (a) Mediterranean and (b) humid-temperate setting.

In the Mediterranean settings, these time lags range from 3 to 4 seasons, and are relatively large (e.g., from wet season 2016 to wet season of 2017, see Fig. 13a). However, in humid-temperate setting, these time lags range from 1 to 3 seasons, mostly owed to the relatively higher precipitation magnitude and frequency in this region (Fig. 13b). In the catchments in both these climate settings, the pulse of sediment leaving the catchment is fairly distributed with the maximum concentration of sediment leaving the catchment in the same wet season when it is eroded from its source. These time-lags would result in enhanced sensitivity of the proportional changes in erosion rates to the changes in seasonal precipitation and (or) vegetation cover, as the sediment is transported even in the seasons when the sediment is not eroded from its source (e.g., wet season in 2017 in both the above climate settings). This poses a limitation to the current study and is again revisited in the model limitations (section 5.5).

5.4 Comparison to previous studies

In this section, we relate the broad findings of this study to the previously published observational studies. In an observational study in an agrarian drainage basin in the Belgian Loam Belt, Steegen et al., (2000) evaluated sediment transport over various time scales (including seasonal). They observed lower sediment fluxes during the seasons with high vegetation cover. In addition, an observational study by Zheng (2006) investigated the effect of vegetation changes on soil erosion in the Loess Plateau, China, and concluded that soil erosion was significantly reduced (up to ~50%) after vegetation restoration. Another observational study in semi-arid grasslands in the Loess Plateau, China, by Hou et al., (2020) highlighted a considerable reduction in erosion rates due to the development of richness and evenness of the plant community in the early to the mid wet season. Our results from scenario 1 (seasonal variations in vegetation cover with constant precipitation rates) support the findings of the above studies whereby a negative correlation (Kendal τ: -0.4 – -0.5) was found between vegetation cover and erosion rates in humid-temperate and Mediterranean settings (see Fig. 5).

Deleted: Pearson r: ~ –

Deleted: 6 and p <

Deleted: 05

Deleted: for the semi-arid

Deleted: . More specifically, we found erosion rates decrease with an increase in vegetation cover in Santa Gracia (semi-arid) and La Campana (Mediterranean) (see Fig. 5). However, a positive correlation (Pearson r: ~0.3 and p<0.05) is observed in the humid-temperate setting from dry season to wet season

A catchment-scale observational study in Baspa Valley, NW Himalayas (Wulf et al., 2010), analyzed seasonal precipitation gradients and their impact on fluvial erosion using weather station observations (1998 – 2007). The study observed a positive correlation between precipitation and sediment yield variability, demonstrating the summer monsoon's first-order control on erosion processes. An observational study by Wei et al., (2015) in Loess Plateau, China, evaluated erosion and sediment transport under various vegetation types and precipitation variations. They found that significant changes in landscape pattern and vegetation coverage (i.e., land use land cover) might contribute to long-term dynamics of soil loss. However, seasonal variations in runoff and sediment yield were mainly influenced by rainfall seasonality. In comparison to the results of this study, we find the similarity in the patterns of erosion rates in scenario 2 (variable precipitation and constant vegetation cover) and scenario 3 (coupled variations in precipitation and vegetation) are consistent with the findings of Wei et al., (2015). For example, the amplitude of change in erosion rates (Fig. 10) in scenarios 2 and 3 differ by 0%, 6%, and –2% in the arid, Mediterranean, and humid-temperate settings, respectively. However, this difference is enhanced in the semi-arid region (i.e., ~23%) due to a relatively high degree of variation (~25%) in seasonal vegetation cover change.

Finally, an observational study in the Columbian Andes by Suescún et al., (2017) assessed the impact of seasonality on vegetation cover and precipitation and found higher erosion rates in regions with steeper slopes. Another study by Chakrapani (2005) emphasized the direct impact of local relief and channel slope on sediment yield in natural rivers. The broad findings of the above studies agree with our results from scenarios 1-3, as we find higher erosion rates in the Mediterranean and humid-temperate regions with steeper topography (mean slope ~20 deg), which encounter high seasonality (and intensity) in precipitation.

5.5. Model Limitations

The model setup used in this study was designed to quantify the sensitivity of erosion rates in different climate and ecological settings with variations in precipitation rates and vegetation cover at seasonal scales. We represent the degree of variations in erosion rates in terms of changes in the amplitude (with respect to the mean) for different model scenarios (see sections 4.1 – 4.3).

Our modeling approach used several simplifying assumptions that warrant discussion and are avenues for investigation in future studies. For example, model results presented here successfully capture the major surface processes, including vegetation-dependent erosion and infiltration, sediment transport, and surface runoff. However, groundwater flow is not considered in the current study, and how the reentry of groundwater into streams over seasonal scales would influence downstream erosion. The reason is that groundwater flow modeling includes a high amount of heterogeneity and anisotropy and requires much finer grid sizes (<1m) and smaller time steps (in seconds to hours). Thus, due to the large grid-cell size (90 m), timescales (monthly), and high uncertainty in subsurface hydrologic parameters we were unable to evaluate the effects of groundwater flow on our results. Furthermore, this study assumed uniform lithologic and hydrologic parameters (e.g., vertical hydraulic conductivity, initial soil moisture, evapotranspiration, erodibility, etc.) over the entire catchment. As said earlier, these properties are subject to a high level of uncertainty and heterogeneity, the best fitting parameters, based on previously published literature (e.g., Schaller et al., 2018; Bernhard et al., 2018; Schmid et al., 2018; Sharma et al., 2021) are used for the model simulations. However, the heterogeneity in vegetation cover and related soil-water infiltration per grid cell is used in this study. For the heterogeneity in vegetation cover, we use MODIS-derived NDVI as a proxy of vegetation cover. According to Garatuza-Payán et al. (2005), NDVI is assumed as an effective tool for estimating seasonal changes in vegetation cover density. However, the spatial resolution (250 m) of the NDVI dataset is lower than that of the SRTM DEM (90 m) used in the study. Nevertheless, the difference in spatial resolution of vegetation cover and topography might introduce ambiguity in the model results. Furthermore, transient dynamics associated with sediment storage in the model is not incorporated in the study to capture the time lag required for the eroded sediment to move out of the model domain. As the LEM (SPACE 1.0) used in

Deleted: soil

Deleted: 4

Deleted: We represent the degree of variations in erosion rates in terms of change amplitude (with respect to the mean) for different model scenarios (see sections 4.1 – 4.3). This study was intended to introduce temporal downscaling (from millennial to seasonal time scales) to the approach of previous similar modeling studies (e.g., Schmid et al., 2018; Sharma et al., 2021).

Deleted: potential

Deleted: lithological

Deleted: hydrological

Deleted: subjected

this study shuffles between detachment- and transport-limited fluvial erosion, we suspect that in such short timescales (3 months) and in small catchments, detachment-limited fluvial erosion is dominant. Hence, any sediment removed from its source is transported out of the domain in a given time-step. However, it is recommended for future studies considering larger or lower gradient catchments, where sediment storage may be more significant than documented here, an analysis of erosion at a local scale (e.g., at individual model grid cells) is recommended.

A final limitation stems from several generalized model parameters (e.g., rock uplift rate, erodibility, diffusivity, etc.) applied to the SRTM DEM (as initial topography). We did this to capture the effects of seasonality in precipitation and vegetation cover in modern times (2000 - 2019). However, the current topography might not have evolved with the same tectonic and lithological parameters. To address this limitation, we conducted simulations for 50 iterations and detrended the model results to remove those transient effects (see section 3.6). This limitation can be handled in future studies by parameterizing the model to the current topography using stochastic (e.g., Bayesian) techniques (e.g., Stephenson et al., 2006; Avdeev et al., 2011). As this study was aimed to capture the control of seasonal precipitation and (or) vegetation changes on the relative variability of erosion rates, the above limitation may not pose a problem in the model results.

6 Summary and Conclusions

In this study, we applied a landscape evolution model to quantify the impact of seasonal variations in precipitation and vegetation on catchment averaged erosion rates. We performed this in regions with varied climate and ecology including: arid, semi-arid, Mediterranean, and humid-temperate settings. Three sets of simulations were designed to model erosion rates for (a) scenario 1: constant precipitation and variable vegetation cover, (b) scenario 2: variable precipitation and constant vegetation cover, and (c) scenario 3: coupled variations in precipitation and vegetation cover. The main conclusions derived from this study are as follows:

1. Scenario 1, with variable vegetation cover and constant precipitation (Fig. 4), resulted in small variations in seasonal erosion rates (<0.02 mm yr^{-1}) in comparison to the other scenarios. The amplitude of change in seasonal erosion rates (relative to the mean) is the smallest in humid-temperate setting and maximum in the Mediterranean setting (Fig. 10a). For example, it ranges from 5% in the arid setting (Pan de Azúcar) to 23% and 36% in the semi-arid (Santa Gracia) and Mediterranean settings (La Campana), respectively.
2. Scenario 2, with constant vegetation cover and variable precipitation (Fig. 6), results in relatively higher seasonal erosion rates (<0.06 mm yr^{-1}) in comparison to scenario 1. The amplitude of change in seasonal erosion rates (relative to the mean) is smallest in the arid setting and largest in the Mediterranean setting (Fig. 10b). For example, it ranges from 13% in the arid setting (Pan de Azúcar) to 52%, 65%, and 91% in the humid-temperate (Nahuelbuta), semi-arid (Santa Gracia), and Mediterranean settings (La Campana), respectively.
3. Scenario 3, with coupled variations in vegetation cover and precipitation (Fig. 8), results in similar seasonal erosion rates (<0.06 mm yr^{-1}) to scenario 2. Similarly, the amplitude of change in seasonal erosion rates (relative to the mean) is the smallest in the arid setting and the largest in the Mediterranean setting (Fig. 10c). For example, it ranges from 13% in the arid setting (Pan de Azúcar) to 50%, 86%, and 97% in the humid-temperate (Nahuelbuta), semi-arid (Santa Gracia), and Mediterranean settings (La Campana), respectively. A significant increase (from scenario 2) in the variation in erosion rates (~21%) is owed to the ~25% variation in vegetation cover in semi-arid settings.
4. All study areas experience maximum and minimum erosion during wet and dry seasons, respectively (Fig. 11b). However, the difference (in maximum and minimum) is amplified from the arid (~30%) to the Mediterranean and humid-temperate settings (~70-75%). This is owed to the range of amplitude of precipitation rate change (Fig. 7) increasing from the arid (e.g., ~9 mm) to humid-temperate settings (e.g., ~543 mm) in wet and dry seasons.

Deleted: simulated the model

Deleted: 6.

Deleted: humid-temperate

Deleted: Nahuelbuta

Deleted: the

Finally, this study was motivated by testing the hypotheses that (1) if precipitation variations primarily influence seasonal erosion, then the influence of seasonal vegetation cover changes would be less significant, and (2) catchment erosion in drier settings is more sensitive to seasonality in precipitation and vegetation, than wetter settings. With respect to hypothesis 1, we found that seasonal precipitation variations primarily drive catchment erosion and the effects of vegetation cover variations are secondary. Results presented here (Fig. 10b) support this interpretation with a high amplitude of change in erosion rates (with respect to means) ranging from 13 to 91% for the scenario with constant vegetation cover and seasonal precipitation variations. However, the effect of seasonal vegetation cover changes is also significant (Fig. 10a), ranging between 5 – 36%. Hence, the first hypothesis is partially confirmed, but the magnitude of response depends on the ecological zone investigated. Concerning hypothesis 2, we found that seasonal changes in catchment erosion are more pronounced in the semi-arid and Mediterranean settings and less pronounced in the arid and humid temperate settings. This interpretation is supported by Fig. 10c, with a significantly high amplitude of change in catchment erosion in semi-arid (~86%) and Mediterranean (~97%) settings with relatively lower changes in humid temperate (~50%) and arid (~13%) settings, partially confirming the hypothesis.

Deleted: significantly

Deleted:)

Appendix A: Input parameters with corresponding units for the landscape evolution model

Table A1. Input parameters with corresponding units for the landscape evolution model

Model Parameters	Values
Grid spacing (dx)	90 m
Model runtime (totalT)	1000 years (2000 - 2019 repeated over 50 times)
time-step (dt)	1 season (3 months)
Rock uplift rate (U)[1]	1.25×10^{-5} [m season^{-1}] (or 0.05 [mm a^{-1}])
Initial sediment thickness (H_initial)[2]	20 (A*), 45 (SA*), 60 (M*), 70 (HT*) [cm]
Bedrock erodibility (Kr)[1]	2×10^{-9} [m^{-1}]
Sediment erodibility (Ks)[1]	2×10^{-8} [m^{-1}]
Reach scale bedrock roughness (H*)[1]	1 [m]
Porosity (Φ)[4]	0.51 (A*), 0.43 (SA*), 0.51 (M*), 0.7 (HT*) [-]
Fraction of fine sediments (Ff)[1]	0.2 [-]
Effective terminal settling velocity (Vs)[1]	2.5 [mm season^{-1}]
m, n[1]	0.6, 1 [-]
Bedrock erosion threshold stream power (ω_cr)[1]	1.25×10^{-5} [m season^{-1}]
Sed. entr. threshold stream power (ω_cs)[1]	1.25×10^{-6} [m season^{-1}]
Bare soil diffusivity (K_b)[1]	2.5×10^{-4} [m2 season^{-1}]
Exponential decay coefficient (α)[1]	0.3 [-]
Critical channel formation area (A_{crit})[3]	1×10^{6} [m^2]
Reference vegetation vover (V_r)[3]	1 (100%)
Manning's number for bare soil (n_s)[3]	0.01 [-]
Manning's number for ref. vegetation (n_v)[3]	0.6 [-]
Scaling factor for vegetation influence (w)[3]	1 [-]
Soil bulk density (B)[4]	1300 (A*), 1500 (SA*), 1300 (M*), 800 (HT*) [kg m^{-3}]
Soil type[4]	sandy loam (A*, SA*, and M*); sandy clay loam (HT*)
Initial soil moisture (s)[5]	0.058 (A*), 0.02 (SA*), 0.053 (M*), 0.15 (HT*) [m^3 m^{-3}]

[1]Sharma et al. (2021), [2]Schaller et al. (2018), [3]Schmid et al. (2018), [4]Bernhard et al. (2018), [5]Übernickel et al. (2020).

Deleted:

Model Parameters
Grid spacing (dx)
Model runtime (totalT)
time-step (dt)
Rock uplift rate (U)[1]
Initial sediment thickness (H_initial)[2]
Bedrock erodibility (Kr)[1]
Sediment erodibility (Ks)[1]
Reach scale bedrock roughness (H*)[1]
Porosity (φ)[1]
Fraction of fine sediments (Ff)[1]
Effective terminal settling velocity (Vs)[1]
m, n[1]
Bedrock erosion threshold stream power (ω_cr
Sed. entr. threshold stream power (ω_cs)[1]
Bare soil diffusivity (K_b)[1]
Exponential decay coefficient (α)[1]
Critical channel formation area (A_{crit})[3]
Reference vegetation cover (V_r)[3]
Manning's number for bare soil (n_s)[3]
Manning's number for ref. vegetation (n_v)[3]
Sacling factor for vegetation influence (w)[3]
Soil bulk density (B)[4]
Soil type[4]
Initial soil moisture (s)[4]

Deleted: [1] Sharma¶

*A: arid; SA: semi-arid; M: Mediterranean; HT: humid-temperate setting.

Appendix B: Implementation of vegetation dependent hillslope and Fluvial processes in Landlab components

This section includes the description of vegetation dependent hillslope and fluvial processes defined in the Landlab components used in this study, based on the approaches by Istanbulluoglu (2005) Schmid et al., (2018), and Sharma et al., (2021).

B1 Vegetation dependent hillslope processes

The rate of change in topography due to hillslope diffusion (Fernandes and Dietrich, 1997) is defined as follows:

$$\frac{\partial z}{\partial t}(hillslope) = \nabla q_s, \quad \text{(A1)}$$

where q_s is sediment flux along the slope S. We applied slope and depth-dependent linear diffusion rule following the approach of Johnstone and Hilley (2014) such that:

$$q_s = K_d S d_* (1 - e^{-H/d_*}), \quad \text{(A2)}$$

where K_d is diffusion coefficient [$m^2\ yr^{-1}$], d_* is sediment transport decay depth [m], and H denotes sediment thickness. The diffusion coefficient is defined as a function of vegetation cover present on hillslopes, which is estimated following the approach of Istanbulluoglu (2005), as follows:

$$K_d = K_b e^{-(\alpha V)}, \quad \text{(A3)}$$

where K_d is defined as a function of vegetation cover V, an exponential decay coefficient α, and linear diffusivity K_b for bare soil.

B2 Vegetation dependent fluvial processes

The fluvial erosion is estimated for a two-layer topography (i.e., bedrock and sediment are treated explicitly) in the coupled detachment– / transport–limited model, SPACE 1.0 (Shobe et al., 2017). Bedrock erosion and sediment entrainment are calculated simultaneously in the model. Total fluvial erosion is defined as:

$$\frac{\partial z}{\partial t}(fluvial) = \frac{\partial R}{\partial t} + \frac{\partial H}{\partial t}, \quad \text{(A4)}$$

where, left-hand side denotes the total fluvial erosion rate. The first and second terms on right-hand side denote the bedrock erosion rate and sediment entrainment rate.
The rate of change of height of bedrock R per unit time [$m\ yr^{-1}$] is defined as:

$$\frac{\partial R}{\partial t} = U - E_r, \quad \text{(A5)}$$

where E_r [$m\ yr^{-1}$], is the volumetric erosion flux of bedrock per unit bed area.
The change in sediment thickness H [m] per unit time [yr] is defined as a fraction net deposition rate and solid fraction sediments, as follows:

$$\frac{\partial H}{\partial t} = \frac{D_s - E_s}{1-\emptyset}, \quad \text{(A6)}$$

where, D_s [$m\ yr^{-1}$] is the deposition flux of sediment, E_s [$m\ yr^{-1}$] is volumetric sediment entrainment flux per unit bed area, and φ is the sediment porosity.

Following the approach of Shobe et al. (2017), E_s and E_r given by:

$$E_s = (K_s q^m S^n - \omega_{cs}) \left(1 - e^{-\frac{H}{H_*}}\right), \quad \text{(A7)}$$

$$E_r = (K_r q^m S^n - \omega_{cr})\, e^{-H/H_*}, \quad \text{(A8)}$$

where, K_s [m^{-1}] and K_r [m^{-1}] are the sediment erodibility and bedrock erodibility parameters respectively. The threshold stream power for sediment entrainment and bedrock erosion are denoted as ω_{cs} [m yr^{-1}] and ω_{cr} [m yr^{-1}] in above equations. Bedrock roughness is denoted as H_* [m] and the term e^{-H/H_*} corresponds to the soil production from bedrock. With higher bedrock roughness magnitudes, more sediment would be produced.

K_s and K_r were modified in the model runtime scripts by introducing the effect of Manning's roughness to quantify the effect of vegetation cover on bed shear stress in each model cell:

$$\tau_v = \rho_w g (n_s + n_v)^{6/10} q^m S^n F_t, \quad \text{(A9)}$$

where, ρ_w [kg m^{-3}] and g [m s^{-2}] are the density of water and acceleration due to gravity respectively. Manning's numbers for bare soil and vegetated surface are denoted as n_s and n_v. F_t represents shear stress partitioning ratio. Manning's number for vegetation cover and F_t are calculated as follows:

$$n_v = n_{vr} \left(\frac{V}{V_r}\right)^w, \quad \text{(A10)}$$

$$F_t = \left(\frac{n_s}{n_s + n_v}\right)^{\frac{3}{2}}, \quad \text{(A11)}$$

where, n_{vr} is Manning's number for the reference vegetation. Here, V_r is reference vegetation cover *(V = 100%)* and V is local vegetation cover in a model cell, w is empirical scaling factor.

By combining stream power equation (Tucker et al., 1999; Howard, 1994; Whipple and Tucker, 1999) and above concept of the effect of vegetation on shear stress, we follow the approach of Schmid et al. (2018) and Sharma et al. (2021) to define new sediment and bedrock erodibility parameters influenced by the surface vegetation cover on fluvial erosion, as follows:

$$K_{vs} = K_s \rho_w g (n_s + n_v)^{6/10} F_t, \quad \text{(A12)}$$

$$K_{vr} = K_r \rho_w g (n_s + n_v)^{6/10} F_t, \quad \text{(A13)}$$

where, K_{vs} [m^{-1}] and K_{vr} [m^{-1}] are modified sediment erodibility and bedrock erodibility respectively. These are influenced by the effect of presence of fraction of vegetation cover V. Hence, K_s and K_r in Eq. (8) and Eq. (9) are replaced by K_{vs} and K_{vr} to include an effect of vegetation cover on fluvial processes in the model. The trends of K_s, K_{vs} and K_{vr} are illustrated in Fig. 3 in Sharma et al., (2021).

Code and data availability

The code and data used in this study are freely available via Zenodo (https://doi.org/10.5281/zenodo.8033782, Sharma and Ehlers, 2023).

Deleted: The code and data used in this study are freely available upon request.¶

Author contributions

HS and TAE designed the initial model setup and simulation programs. HS and TAE conducted model modifications, simulation runs, and analysis. HS prepared the paper with contributions from TAE.

Competing interests

The authors declare that they have no conflict of interest.

Acknowledgments

We acknowledge the support from the Open Access Publishing fund of the University of Tübingen. We would like to thank two anonymous reviewers and Omer Yetemen for their constructive reviews. We also thank Simon Mudd for editing this paper.

Financial support

This research has been supported by the Deutsche Forschungs Gemeinschaft (grant nos. EH329/14-2, SPP-1803, and Research Training Group 1829 Integrated Hydrosystem Modelling).

Review Statement

This paper was edited by Simon Mudd and reviewed by two anonymous reviewers and Omer Yetemen.

Deleted: Hemanti Sharma and Todd A. Ehlers

Deleted: Fund

Deleted: acknowledge

Formatted: Font: Bold, Font color: Auto

Deleted: from the

Formatted: Font color: Auto,

Deleted:

Formatted: Font color: Auto,

Deleted: , funded by the German Research Foundation (DFG). In addition, Todd A. Ehlers acknowledges support from the German priority research program "EarthShape: Earth Surface Shaping

Formatted: Font color: Auto,

Deleted: Biota" (SPP-1803; EH329/14-2). We thank xxx and yyy for their constructive reviews

Formatted: Font color: Auto,

Formatted

References

Avdeev, B., Niemi, N. A., and Clark, M. K.: Doing more with less: Bayesian estimation of erosion models with detrital thermochronometric data, Earth Planet. Sci. Lett., 305, 385–395, https://doi.org/10.1016/j.epsl.2011.03.020, 2011.

Barnhart, K. R., Glade, R. C., Shobe, C. M., and Tucker, G. E.: Terrainbento 1.0: a Python package for multi-model analysis in long-term drainage basin evolution, Geosci. Model Dev., 12, 1267–1297, https://doi.org/10.5194/gmd-12-1267-2019, 2019.

Beaudoing, H., Rodell, M., and NASA/GSFC/HSL: GLDAS Noah Land Surface Model L4 monthly 0.25 x 0.25 degree, Version 2.1, https://doi.org/10.5067/SXAVCZFAQLNO, 2020.

Bernhard, N., Moskwa, L.-M., Schmidt, K., Oeser, R. A., Aburto, F., Bader, M. Y., Baumann, K., von Blanckenburg, F., Boy, J., van den Brink, L., Brucker, E., Büdel, B., Canessa, R., Dippold, M. A., Ehlers, T. A., Fuentes, J. P., Godoy, R., Jung, P., Karsten, U., Köster, M., Kuzyakov, Y., Leinweber, P., Neidhardt, H., Matus, F., Mueller, C. W., Oelmann, Y., Oses, R., Osses, P., Paulino, L., Samolov, E., Schaller, M., Schmid, M., Spielvogel, S., Spohn, M., Stock, S., Stroncik, N., Tielbörger, K., Übernickel, K., Scholten, T., Seguel, O., Wagner, D., and Kühn, P.: Pedogenic and microbial interrelations to regional climate and local topography: New insights from a climate gradient (arid to humid) along the Coastal Cordillera of Chile, CATENA, 170, 335–355, https://doi.org/10.1016/j.catena.2018.06.018, 2018.

Bookhagen, B., Thiede, R. C., and Strecker, M. R.: Abnormal monsoon years and their control on erosion and sediment flux in the high, arid northwest Himalaya, Earth Planet. Sci. Lett., 231, 131–146, https://doi.org/10.1016/j.epsl.2004.11.014, 2005.

Brown, C. E.: Coefficient of Variation, in: Applied Multivariate Statistics in Geohydrology and Related Sciences, Springer, Berlin, Heidelberg, 1998.

Buendia, C., Vericat, D., Batalla, R. J., and Gibbins, C. N.: Temporal Dynamics of Sediment Transport and Transient In-channel Storage in a Highly Erodible Catchment: LINKING SEDIMENT SOURCES, RAINFALL PATTERNS AND SEDIMENT YIELD, Land Degrad. Dev., 27, 1045–1063, https://doi.org/10.1002/ldr.2348, 2016.

Carretier, S., Tolorza, V., Regard, V., Aguilar, G., Bermúdez, M. A., Martinod, J., Guyot, J.-L., Hérail, G., and Riquelme, R.: Review of erosion dynamics along the major N-S climatic gradient in Chile and perspectives, Geomorphology, 300, 45–68, https://doi.org/10.1016/j.geomorph.2017.10.016, 2018.

Cerdà, A.: The influence of aspect and vegetation on seasonal changes in erosion under rainfall simulation on a clay soil in Spain, Can. J. Soil Sci., 78, 321–330, https://doi.org/10.4141/S97-060, 1998.

Chakrapani, G. J.: Factors controlling variations in river sediment loads, Curr. Sci., 88, 569–575, 2005.

Deal, E., Favre, A. C., and Braun, J.: Rainfall variability in the Himalayan orogen and its relevance to erosion processes: RAINFALL VARIABILITY IN THE HIMALAYAS, Water Resour. Res., 53, 4004–4021, https://doi.org/10.1002/2016WR020030, 2017.

Didan, Kamel: MOD13Q1 MODIS/Terra Vegetation Indices 16-Day L3 Global 250m SIN Grid V006, https://doi.org/10.5067/MODIS/MOD13Q1.006, 2015.

Earth Resources Observation And Science (EROS) Center: Shuttle Radar Topography Mission (SRTM) Void Filled, https://doi.org/10.5066/F7F76B1X, 2017.

Fernandes, N. F. and Dietrich, W. E.: Hillslope evolution by diffusive processes: The timescale for equilibrium adjustments, Water Resour. Res., 33, 1307–1318, https://doi.org/10.1029/97wr00534, 1997.

Ferreira, V. and Panagopoulos, T.: Seasonality of Soil Erosion Under Mediterranean Conditions at the Alqueva Dam Watershed, Environ. Manage., 54, 67–83, https://doi.org/10.1007/s00267-014-0281-3, 2014.

Gabarrón-Galeote, M. A., Martínez-Murillo, J. F., Quesada, M. A., and Ruiz-Sinoga, J. D.: Seasonal changes in the soil hydrological and erosive response depending on aspect, vegetation type and soil water repellency in different Mediterranean microenvironments, Solid Earth, 4, 497–509, https://doi.org/10.5194/se-4-497-2013, 2013.

Gao, P., Li, Z., and Yang, H.: Variable discharges control composite bank erosion in Zoige meandering rivers, CATENA, 204, 105384, https://doi.org/10.1016/j.catena.2021.105384, 2021.

Garatuza-Payán, J., Sánchez-Andrés, R., Sánchez-Carrillo, S., and Navarro, J. M.: Using remote sensing to investigate erosion rate variability in a semiarid watershed, due to changes in vegetation cover, IAHS Publ, 292, 144–151, 2005.

Glodny, J., Gräfe, K., Echtler, H., and Rosenau, M.: Mesozoic to Quaternary continental margin dynamics in South-Central Chile (36–42°S): the apatite and zircon fission track perspective, Int. J. Earth Sci., 97, 1271–1291, https://doi.org/10.1007/s00531-007-0203-1, 2008.

Green, W. H. and Ampt, G. A.: Studies on Soil Phyics., J. Agric. Sci., 4, 1–24, https://doi.org/10.1017/S0021859600001441, 1911.

Hancock, G. and Lowry, J.: Hillslope erosion measurement—a simple approach to a complex process, Hydrol. Process., 29, 4809–4816, 2015.

Hancock, G. and Lowry, J.: Quantifying the influence of rainfall, vegetation and animals on soil erosion and hillslope connectivity in the monsoonal tropics of northern Australia, Earth Surf. Process. Landf., 46, 2110–2123, https://doi.org/10.1002/esp.5147, 2021.

Herrmann, S. M. and Mohr, K. I.: A Continental-Scale Classification of Rainfall Seasonality Regimes in Africa Based on Gridded Precipitation and Land Surface Temperature Products, J. Appl. Meteorol. Climatol., 50, 2504–2513, https://doi.org/10.1175/JAMC-D-11-024.1, 2011.

Hobley, D. E. J., Adams, J. M., Nudurupati, S. S., Hutton, E. W. H., Gasparini, N. M., Istanbulluoglu, E., and Tucker, G. E.: Creative computing with Landlab: an open-source toolkit for building, coupling, and exploring two-dimensional numerical models of Earth-surface dynamics, Earth Surf. Dyn., 5, 21–46, https://doi.org/10.5194/esurf-5-21-2017, 2017.

Hou, J., Zhu, H., Fu, B., Lu, Y., and Zhou, J.: Functional traits explain seasonal variation effects of plant communities on soil erosion in semiarid grasslands in the Loess Plateau of China, Catena, v. 194, 104743-, https://doi.org/10.1016/j.catena.2020.104743, 2020.

Howard, A. D.: A detachment-limited model of drainage basin evolution, Water Resour. Res. V 30, 2261–2285, 1994.

Huete, A., Didan, K., Miura, T., Rodriguez, E. P., Gao, X., and Ferreira, L. G.: Overview of the radiometric and biophysical performance of the MODIS vegetation indices, Remote Sens. Environ., 83, 195–213, https://doi.org/10.1016/S0034-4257(02)00096-2, 2002.

Istanbulluoglu, E.: Vegetation-modulated landscape evolution: Effects of vegetation on landscape processes, drainage density, and topography, J. Geophys. Res., 110, https://doi.org/10.1029/2004jf000249, 2005.

Istanbulluoglu, E. and Bras, R. L.: On the dynamics of soil moisture, vegetation, and erosion: Implications of climate variability and change, Water Resour. Res., 42, 2006.

Johnstone, S. A. and Hilley, G. E.: Lithologic control on the form of soil-mantled hillslopes, Geology, 43, 83–86, https://doi.org/10.1130/G36052.1, 2014.

Julien, P. Y., Saghafian, B., and Ogden, F. L.: RASTER-BASED HYDROLOGIC MODELING OF SPATIALLY-VARIED SURFACE RUNOFF1, JAWRA J. Am. Water Resour. Assoc., 31, 523–536, https://doi.org/10.1111/j.1752-1688.1995.tb04039.x, 1995.

Langbein, W. B. and Schumm, S. A.: Yield of sediment in relation to mean annual precipitation, Eos Trans. Am. Geophys. Union, 39, 1076–1084, https://doi.org/10.1029/TR039i006p01076, 1958.

Leyland, J., Hackney, C. R., Darby, S. E., Parsons, D. R., Best, J. L., Nicholas, A. P., Aalto, R., and Lague, D.: Extreme flood-driven fluvial bank erosion and sediment loads: direct process measurements using integrated Mobile Laser Scanning (MLS) and hydro-acoustic techniques: Direct measurement of flood-driven erosion using MLS and MBES, Earth Surf. Process. Landf., 42, 334–346, https://doi.org/10.1002/esp.4078, 2016.

Melnick, D.: Rise of the central Andean coast by earthquakes straddling the Moho, Nat. Geosci., 9, 401–407, https://doi.org/10.1038/ngeo2683, 2016.

Melnick, D., Bookhagen, B., Strecker, M. R., and Echtler, H. P.: Segmentation of megathrust rupture zones from fore-arc deformation patterns over hundreds to millions of years, Arauco peninsula, Chile: EARTHQUAKE SEGMENTATION AT ARAUCO, J. Geophys. Res. Solid Earth, 114, https://doi.org/10.1029/2008JB005788, 2009.

Mosaffaie, J., Ekhtesasi, M. R., Dastorani, M. T., Azimzadeh, H. R., and Zare Chahuki, M. A.: Temporal and spatial variations of the water erosion rate, Arab. J. Geosci., 8, 5971–5979, https://doi.org/10.1007/s12517-014-1628-z, 2015.

Oeser, R. A., Stroncik, N., Moskwa, L.-M., Bernhard, N., Schaller, M., Canessa, R., Brink, L. van den, Köster, M., Brucker, E., Stock, S., Fuentes, J. P., Godoy, R., Matus, F. J., Pedraza, R. O., McIntyre, P. O., Paulino, L., Seguel, O., Bader, M. Y., Boy, J., Dippold, M. A., Ehlers, T. A., Kühn, P., Kuzyakov, Y., Leinweber, P., Scholten, T., Spielvogel, S., Spohn, M., Übernickel, K., Tielbörger, K., Wagner, D., and Blanckenburg, F. von: Chemistry and microbiology of the Critical Zone along a steep climate and vegetation gradient in the Chilean Coastal Cordillera, CATENA, 170, 183–203, https://doi.org/10.1016/j.catena.2018.06.002, 2018.

Rengers, F. K., McGuire, L., Kean, J. W., Staley, D. M., and Hobley, D. E. J.: Model simulations of flood and debris flow timing in steep catchments after wildfire, Water Resour. Res., 52, 6041–6061, https://doi.org/10.1002/2015WR018176, 2016.

Rodell, M., Houser, P. R., Jambor, U., Gottschalck, J., Mitchell, K., Meng, C.-J., Arsenault, K., Cosgrove, B., Radakovich, J., Bosilovich, M., Entin, J. K., Walker, J. P., Lohmann, D., and Toll, D.: The Global Land Data Assimilation System, Bull. Am. Meteorol. Soc., 85, 381–394, https://doi.org/10.1175/BAMS-85-3-381, 2004.

Schaller, M. and Ehlers, T. A.: Comparison of soil production, chemical weathering, and physical erosion rates along a climate and ecological gradient (Chile) to global observations, Earth Surf. Dyn., 10, 131–150, https://doi.org/10.5194/esurf-10-131-2022, 2022.

Schaller, M., Ehlers, T. A., Lang, K. A. H., Schmid, M., and Fuentes-Espoz, J. P.: Addressing the contribution of climate and vegetation cover on hillslope denudation, Chilean Coastal Cordillera (26°–38°S), Earth Planet. Sci. Lett., 489, 111–122, https://doi.org/10.1016/j.epsl.2018.02.026, 2018.

Schaller, M., Dal Bo, I., Ehlers, T. A., Klotzsche, A., Drews, R., Fuentes Espoz, J. P., and van der Kruk, J.: Comparison of regolith physical and chemical characteristics with geophysical data along a climate and ecological gradient, Chilean Coastal Cordillera (26 to 38\degree\,S), SOIL, 6, 629–647, https://doi.org/10.5194/soil-6-629-2020, 2020.

Schmid, M., Ehlers, T. A., Werner, C., Hickler, T., and Fuentes-Espoz, J.-P.: Effect of changing vegetation and precipitation on denudation – Part 2: Predicted landscape response to transient climate and vegetation cover over millennial to million-year timescales, Earth Surf. Dyn., 6, 859–881, https://doi.org/10.5194/esurf-6-859-2018, 2018.

Sharma and Ehlers: LandLab investigations into the seasonal effects of precipitation and vegetation change on catchment erosion, , https://doi.org/10.5281/zenodo.8033782, 2023.

Sharma, H., Ehlers, T. A., Glotzbach, C., Schmid, M., and Tielbörger, K.: Effect of rock uplift and Milankovitch timescale variations in precipitation and vegetation cover on catchment erosion rates, Earth Surf. Dyn., 9, 1045–1072, https://doi.org/10.5194/esurf-9-1045-2021, 2021.

Shobe, C. M., Tucker, G. E., and Barnhart, K. R.: The SPACE 1.0 model: A Landlab component for 2-D calculation of sediment transport, bedrock erosion, and landscape evolution, Geosci. Model Dev. Discuss., 1–38, https://doi.org/10.5194/gmd-2017-175, 2017.

Starke, J., Ehlers, T. A., and Schaller, M.: Latitudinal effect of vegetation on erosion rates identified along western South America, Science, 367, 1358–1361, https://doi.org/10.1126/science.aaz0840, 2020.

Steegen, A., Govers, G., Nachtergaele, J., Takken, I., Beuselinck, L., and Poesen, J.: Sediment export by water from an agricultural catchment in the Loam Belt of central Belgium, Geomorphology, 33, 25–36, https://doi.org/10.1016/S0169-555X(99)00108-7, 2000.

Stephenson, J., Gallagher, K., and Holmes, C.: A Bayesian approach to calibrating apatite fission track annealing models for laboratory and geological timescales, Geochim. Cosmochim. Acta, 70, 5183–5200, https://doi.org/10.1016/j.gca.2006.07.027, 2006.

Suescún, D., Villegas, J. C., León, J. D., Flórez, C. P., García-Leoz, V., and Correa-Londoño, G. A.: Vegetation cover and rainfall seasonality impact nutrient loss via runoff and erosion in the Colombian Andes, Reg. Environ. Change, 17, 827–839, https://doi.org/10.1007/s10113-016-1071-7, 2017.

Tucker, G. E. and Bras, R. L.: A stochastic approach to modeling the role of rainfall variability in drainage basin evolution, Water Resour. Res., 36, 1953–1964, https://doi.org/10.1029/2000wr900065, 2000.

Tucker, G. E., Gasparini, N. M., Lancaster, S. T., and Bras, R. L.: Modeling Floodplain Dynamics and Stratigraphy: Implications for Geoarchaeology, 1999.

Übernickel, K., Ehlers, T. A., Ershadi, M. R., Paulino, L., Fuentes Espoz, J.-P., Maldonado, A., Oses-Pedraza, R., and von Blanckenburg, F.: Time series of meteorological station data in the EarthShape study areas of in the Coastal Cordillera, Chile, https://doi.org/10.5880/FIDGEO.2020.043, 2020.

Wang, L., Zheng, F., Liu, G., Zhang, X. J., Wilson, G. V., Shi, H., and Liu, X.: Seasonal changes of soil erosion and its spatial distribution on a long gentle hillslope in the Chinese Mollisol region, Int. Soil Water Conserv. Res., 9, 394–404, https://doi.org/10.1016/j.iswcr.2021.02.001, 2021.

Wei, W., Chen, L., Zhang, H., and Chen, J.: Effect of rainfall variation and landscape change on runoff and sediment yield from a loess hilly catchment in China, Environ. Earth Sci., 73, 1005–1016, https://doi.org/10.1007/s12665-014-3451-y, 2015.

Whipple, K. X. and Tucker, G. E.: Dynamics of the stream-power river incision model: Implications for height limits of mountain ranges, landscape response timescales, and research needs, J. Geophys. Res. Solid Earth, 104, 17661–17674, https://doi.org/10.1029/1999jb900120, 1999.

Wulf, H., Bookhagen, B., and Scherler, D.: Seasonal precipitation gradients and their impact on fluvial sediment flux in the Northwest Himalaya, Geomorphology, 118, 13–21, https://doi.org/10.1016/j.geomorph.2009.12.003, 2010.

Yetemen, O., Istanbulluoglu, E., Flores-Cervantes, J. H., Vivoni, E. R., and Bras, R. L.: Ecohydrologic role of solar radiation on landscape evolution, Water Resour. Res., 51, 1127–1157, https://doi.org/10.1002/2014wr016169, 2015.

Zhang, S., Li, Z., Hou, X., and Yi, Y.: Impacts on watershed-scale runoff and sediment yield resulting from synergetic changes in climate and vegetation, Catena, 179, 129–138, https://doi.org/10.1016/j.catena.2019.04.007, 2019.

Zhang, W., An, S., Xu, Z., Cui, J., and Xu, Q.: The impact of vegetation and soil on runoff regulation in headwater streams on the east Qinghai–Tibet Plateau, China, Catena, 87, 182–189, https://doi.org/10.1016/j.catena.2011.05.020, 2011.

Zhang, X., Yu, G. Q., Li, Z. B., and Li, P.: Experimental Study on Slope Runoff, Erosion and Sediment under Different Vegetation Types, Water Resour. Manag., 28, 2415–2433, https://doi.org/10.1007/s11269-014-0603-5, 2014.

Zheng, F. L.: Effect of Vegetation Changes on Soil Erosion on the Loess Plateau1 1Project supported by the Chinese Academy of Sciences (No. KZCX3-SW-422) and the National Natural Science Foundation of China (Nos. 9032001 and 40335050)., Pedosphere, 16, 420–427, https://doi.org/10.1016/S1002-0160(06)60071-4, 2006.

188 Ziese, M., Rauthe-Schöch, A., Becker, A., Finger, P., Rustemeier, E., and Schneider, U.: GPCC Full Data Daily Version 2020
189 at 1.0°: Daily Land-Surface Precipitation from Rain-Gauges built on GTS-based and Historic Data: Gridded Daily Totals
190 (2020), https://doi.org/10.5676/DWD_GPCC/FD_D_V2020_100, 2020.

191